Validation of actinometry for estimating relative hydrogen atom densities and electron energy evolution in plasma assisted diamond deposition reactors

A. Gicquel
Laboratoire d'Ingéniérie des Matériaux et des Hautes Pressions, CNRS-UPR 1311-Université Paris-Nord, Avenue J. B. Clément 93430, Villetaneuse France

M. Chenevier
Laboratoire de spectrométrie Physique, CNRS-UMR C5588, Université Joseph Fourier de Grenoble, B.P.87, 38402, Saint Martin d'Hères Cedex, France

Kh. Hassouni
Laboratoire d'Ingéniérie des Matériaux et des Hautes Pressions, CNRS-UPR 1311-Université Paris-Nord, Avenue J. B. Clément 93430, Villetaneuse France

A. Tserepi
Laboratoire de spectrométrie Physique, CNRS-UMR C5588, Université Joseph Fourier de Grenoble, B.P.87, 38402, Saint Martin d'Hères Cedex, France

M. Dubus
Laboratoire d'Ingéniérie des Matériaux et des Hautes Pressions, CNRS-UPR 1311-Université Paris-Nord, Avenue J. B. Clément 93430, Villetaneuse, France

(Received 9 April 1997; accepted for publication 5 March 1998)

The validity of the actinometry method applied to H-atom mole fraction measurements has been analyzed. First, a theoretical approach allowed us to determine boundary conditions for which the validity of actinometry may be critical. For these specific conditions, corresponding to an upper limit of electron temperature of 20 000 K and a lower limit of H-atom mole fraction of 2%–4%, spatial distributions of the ground state H-atom relative densities provided either by two photon allowed transition or by optical emission spectroscopy (OES) were compared and seen to be proportional. This proves that the H atoms excited in the level of quantum number $n=3$ (level used for OES experiments) are produced directly from the ground electronic state during collisions with electrons. Actinometry can then be applied under these experimental conditions. Second, the emission intensity ratio of two lines issued from excited states of argon was demonstrated to be indirectly related to the ''electron temperature'' of the hot electrons of the plasma. This allowed us to predict the way of evolution of the plasma electrons' energy as a function of the operating conditions. Thus, experiments (which have been confirmed by calculations) showed that the electron energy decreases as a function of the microwave power density and remains constant as a function of the methane percentage introduced in the feed gas at least up to 6%. The consequence is that the domain of diamond deposition discharge conditions for which actinometry is valid is quite wide. Once the microwave volumetric power density is more than $9\ \mathrm{W\ cm^{-3}}$, and the percentage of methane less than 6%, actinometry can be applied. However, the estimation of variations of H-atom mole fractions as a function of the operating conditions implies the use of correcting factors, which are discussed. They are mainly due to the large influence of the quenching processes under these experimental conditions. An experimental estimate of the quenching cross section of the H($n=3$) atoms by ground state molecular hydrogen, which was unknown and involved in the correcting factors, is presented. Finally, relative variations of H-atom mole fraction in space and as a function of the methane percentage are shown. © *1998 American Institute of Physics.*
[S0021-8979(98)06111-8]

I. INTRODUCTION

Optical emission spectroscopy (OES) can be a very powerful technique for indirectly accessing ground electronic state species concentrations and temperatures, and for better understanding the processes occuring in a plasma. However, measurements made by OES have to be interpreted carefully. As a matter of fact, OES only provides measurements of species in electronic excited states which participate only in a minor proportion to the plasma or plasma/surface chemistry and which are at a concentration level of less than 10^{-4} with respect to species in the electronic ground state. Extracting information concerning the plasma processes by measuring relative concentrations and temperatures from OES implies the establishment of relationships between species in electronic excited states (analyzed by OES) and those in the electronic ground state (which generally include the key spe-

cies for the studied process). For instance, temperatures (vibration, translation, rotation) measured on electronic excited states must be compared to those measured on electronic ground state using laser diagnostics. Concerning the concentration measurements, Coburn and Chen,[1] in the early 80's, have introduced the actinometry technique which offers the possibility of reaching relative concentrations of a ground state species from emission intensity measurements. Actinometry requires the introduction of a gas as an impurity in the feed gas, and this minor impurity constitutes the actinometer. The actinometer compensates for changes in the electron density or energy, and then plays a normalization role for the species' emission intensity. If actinometry is valid, then the emission intensity ratio (species over actinometer) is proportional to the species electronic ground state relative concentration. The conditions of validity of this technique are rather restrictive, and have to be carefully analyzed before any use. In particular, (i) both the actinometer and the studied species must be excited from their electronic ground state through an electron impact; (ii) the excitation cross sections of these processes must have the same energy threshold and must be proportional for the range of electron energy corresponding to the discharge conditions (same shape of the cross sections); (iii) the excited species loss must be dominated by radiative processes. If condition (iii) is not met, additional loss terms (due to quenching processes, for instance) must be taken into account.

Laser diagnostics, available today in different laboratories, allow direct probing of the species in their ground electronic states. However, they are expensive, nonflexible, and require special windows which may create undesirable changes in the electric field distribution inside the reactor, and thus in the plasma characteristics. We have observed this behavior in a microwave plasma reactor working with a resonant cavity coupling configuration. Owing to these requirements, a very large range of experimental conditions can rarely be tested. In addition, laser techniques are not appropriate for monitoring industrial reactors.

Titration, laser spectroscopies, and optical absorption spectroscopies all can be used for assessing the validity of actinometry. The simultaneous use of OES and laser diagnostics provides a unique possibility of studying at the laboratory scale the excitation processes of the plasma species, and for establishing the relationship linking ground and excited electronic state species concentrations. This procedure is appropriate to determine the domain of validity of actinometry, under specific ranges of conditions. Once the relationships are found, then emission spectroscopy alone may be used for monitoring plasma processes and studying plasma parameters. Calibration techniques involving titration, absorption spectroscopy, or modeling are appropriate for reaching absolute measurements.

Such an approach has been already used for studying different kinds of plasmas.[2–7] Gottscho *et al.*[5] have thus studied the mechanisms of production Cl and F atoms in $CF_4/O_2/Ar$ and Cl_2/Ar plasmas, and Walkup *et al.*[6] the production of oxygen atoms in O_2+CF_4 rf discharges. By comparing laser absorption spectroscopy and OES results, Gicquel *et al.*[7] showed that electronic excited $NH(A^3\Pi)$ radicals are produced from the electronic ground state by direct electron impact in the volume of a radio-frequency low pressure discharge of NH_3 but not at the plasma/surface interface where a cathodic sheath was observed (very high electron energy).

Owing to the important role of H atoms and CH_3 radicals in controlling chemical vapor deposited (CVD) diamond films' quality and growth rates,[8–14] the knowledge of their concentrations, as well as their production and consumption governing parameters, is crucial. As shown previously,[15–17] H-atom production rate is a function, in diamond deposition plasma reactors, of both electron temperature and gas temperature, which control, respectively, electron impact dissociation and thermal dissociation of molecular hydrogen. The atoms' destruction is partly due to the dissociation in volume of CH_4 and CH_3 species via collisional reactions,[15,18–20] which occur at relatively high gas temperatures. It is also due to surface (walls, diamond surface) reactions such as etching and catalytic surface recombination processes.[8,15,17,21–24] At high pressure, volume recombination reactions may become important. Measurements of relative H-atom concentration and temperatures have already been reported in hot filament and plasma reactors using mass spectrometry,[14] resonance enhanced multiphoton ionization (REMPI),[25] third harmonic generation (THG),[26] coherent anti-Stokes raman spectroscopy (CARS),[15,18,41] two photon allowed transition laser induced fluorescence (TALIF),[27–32] and OES.[15,30–40,42] Several absolute measurements of H-atom mole fraction were obtained in hot filament reactors and only few in moderate pressure microwave plasma reactors.[14,30]

Actinometry has been used in the past for determining H-atom concentration variation,[15,33,34,37] however, to our knowledge, a detailed analysis on the validity of actinometry for H-atom under diamond deposition conditions has not yet been reported. The validity of actinometry for H atom has been discussed in Refs. 35, 36, 37, and 38, but for operating conditions far from those corresponding to diamond deposition. In particular, in these latter cases, the pressure was low enough to neglect the quenching of the excited species by the main ground state species.

The goals of this article are (i) to draw the domain of validity of actinometry for H atoms in diamond deposition microwave plasma reactors (pressure between 1000 and 20 000 Pa, electron temperature less than 20 000 K), (ii) to estimate spatial distributions of relative H-atom densities, and (iii) to analyze their variations as a function of the percentage of methane introduced in the feed gas up to 6% (typical for diamond deposition).

In the first part of the article, we analyze theoretically the production and loss terms of excited H atoms (in particular the H atoms excited in the level of quantum number $n=3$) as a function of electron temperature, H-atom mole fraction, and pressure on the basis of the literature data. By comparing the relative contributions of different paths leading to $H(n=3)$, we find local boundary conditions in terms of electron temperature and H-atom mole fraction for which the validity of actinometry may be critical. We then relate these local boundary conditions to macroscopic parameters in terms of microwave power density and percentage of

methane introduced in the feed gas. Then, we establish the relationship linking H-atom mole fraction to emission intensity measurements. In this part, we also examine the role of the quenching reactions in affecting the populations of excited species. In particular, the quenching cross sections of the radiative electronic excited Ar($4p$) state ($2p_1$ and $2p_9$ sublevels in Paschen notation) by molecular hydrogen are estimated experimentally.

In a second part of the article, the validity of actinometry for H atoms is demonstrated experimentally for the conditions corresponding to the boundary (limit local conditions) found above. For these conditions, by comparing TALIF and OES results, we demonstrate that the $n=3$ electronic excited state of H atom is produced from the ground electronic state by a direct electron impact.

Finally, in the third part, in order to draw the domain of conditions for which actinometry should be valid, we use experiments as well as a one-dimensional (1D) diffusive H_2 plasma flow model developed in the laboratory, for estimating the variations of the local plasma parameters (electron energy, gas temperature, H-atom mole fraction) as functions of the operating conditions (power density, percentage of methane). For instance, we gain insight into the fact that with increasing pressure and power simultaneously, the electron temperature decreases while the H-atom mole fraction increases.

II. EXPERIMENTAL SETUP AND DIAGNOSTICS

A. Microwave reactor

The microwave plasma diamond deposition reactor, made of a silica bell jar, operates under moderate pressure. The detailed description of the deposition device has already been presented elsewhere.[15] The feed gas is a mixture of a few percent methane (0–5%) in hydrogen, as conventionally used for diamond deposition. The feed gas is activated by either a 1200 W or a 6 kW, 2.45 GHz SAIREM microwave generator. Some 5 cm-diam ⟨100⟩ single crystal silicon wafers covered by a polycrystalline untextured diamond film were always placed inside the plasma ball. Then, the study concerns a H_2+CH_4 plasma interacting with an untextured diamond surface.

The averaged input microwave power density, defined as the ratio of the input microwave power over the volume of the plasma obtained in the absence of substrate holder (plasma ball) (in W cm^{-3}) was changed by a simultaneous variation of the pressure and the microwave power, while keeping the plasma volume constant as much as possible. The plasma volume and the ratio of the power to the total density (P_{MW}/n) (where P_{MW} is the injected power in W and n, the total density, in cm^{-3}) were kept constant. Their corresponding values are, respectively, 65 cm^3 and between 6 and 7×10^{-15} W cm^{-3}/mol. The power was varied from 400 to 2400 W, and the pressure from 800 to 14 000 Pa. The corresponding variation range of the power density is 4.5–37 W cm^{-3}. The uncertainties on the plasma volume and on the averaged power density (in W cm^{-3}) were estimated at around 2% and 10%, respectively. The uncertainty on the volume is eventually weak owing to the fact that most of the power is dissipated is a central region and not equally in the whole plasma volume.

Depending on the plasma conditions, in particular the averaged microwave power density, heating or cooling of the substrate holder was used to maintain the substrate temperature constant at 900 °C.

B. Two photon allowed transition LIF (TALIF) technique

Two photon allowed transition laser induced fluorescence (TALIF) measurements were conducted in the reactor equipped with two UV grade silica windows allowing transmission of 205 nm of light. The whole reactor was accurately translated vertically and horizontally with respect to the laser beam in order to obtain axial and radial profiles. The spatial resolution is estimated at 0.5 mm axially and 1 mm radially. The whole setup has been presented in detail elsewhere.[28,32]

Briefly, the system used to generate the light at about 205 nm consists of a pulsed excimer laser (XeCl) emitting at 308 nm. This excimer pumps a dye laser composed of a tunable oscillator and an amplifier. With rhodamine B an intense beam is obtained at 615 nm which is frequency doubled in a potassium dihydrogen phosphate (KDP) crystal to give 307.5 nm. Mixing with the residual beam at 615 nm in a BBO crystal produces the 205 nm beam, with a repetition rate of 10 Hz and a pulse duration of about 25 ns. The energy and the linewidth are typically of 50 μJ per pulse and 0.0025 nm, respectively. The whole laser system is computer controlled and allows wavelength scanning over a few nm. In our experiment a scan of 0.030 nm is sufficient to cover the line profile with 90 steps. The profile line is obtained with a laser wavelength varying from 205.065 to 205.095 nm, allowing the doubled $1^2S\rightarrow3^2S(^2D)$ H atom transition to occur (with $\lambda_0=205.14$ nm in vacuum and 205.082 in air). The fluorescence light, provided by the transition towards $n=2$ H-atom electronic state, is collected at 90° to the laser beam by two lenses. It is detected directly by a photomultiplier in front of which an interference filter centered at 656.5 nm is used to eliminate scattered laser light. The resulting signal is processed by a boxcar integrator and sent to a computer. The fluorescence signal is averaged over 20 laser shots for each wavelength step, thus a scan takes about 3 min. Under the experimental conditions, the observed two photon line profile is Doppler broadening dominated. Its full width at half maximum is directly related to the translational temperature of the atoms, and its area to their concentration.

C. Optical emission spectroscopy (OES)

A Jobin Yvon THR 1000 spectrometer mounted with a 1800 groves per mm grating, blazed at 450 nm and equipped with a photomultiplier (Hamamatsu R 3896) and a red region intensified OMA III (EGG-Princeton Instrument-1460) was used to perform emission spectroscopy. The light emitted from the plasma was collected by a 1 ML optical collimator and transported via an optical fiber to the entrance slit of the monochromator. This device enables a spatial resolution in the plasma emissive cylinder of approximately 2 mm in di-

ameter. The optical system was mounted on a computer controlled motion table, allowing axial and radial measurements. Emission intensity profiles, averaged on the line of sight, were measured at 90° to the axis of the reactor. An Abel inversion procedure was applied on these profiles in order to obtain radial distributions of the emission intensity of the excited species.[42] At a given axial location in the plasma, as the plasma volume is kept constant when changing the operating conditions, the line-of-sight averaged emission intensities are always measured within the same plasma volume.

The emission intensities of H_α ($\lambda = 656.5$ nm), H_β ($\lambda = 486.1$ nm), and H_γ ($\lambda = 432.1$ nm) were recorded systematically using the optical multichannel analyzer. Argon was introduced at 1% in the plasma and the $4p \rightarrow 4s$ argon transitions [$\lambda = 750.3$ nm ($2p_1 \rightarrow 1s_2$) and $\lambda = 811.5$ nm ($2p_9 \rightarrow 1s_5$)] (in Paschen notation) were measured.

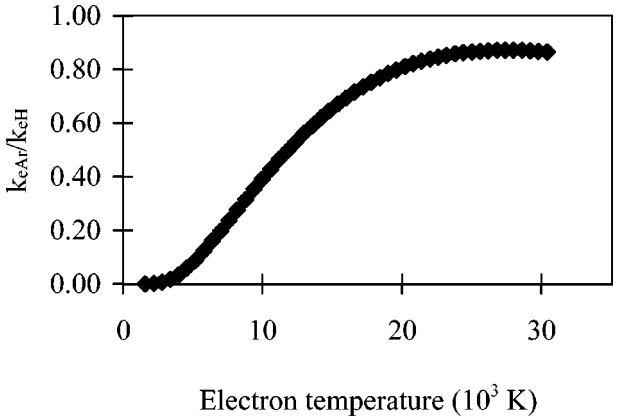

FIG. 1. Variations of the ratio of electron excitation rate constants of Ar($4p$) ($2p_1$ state in Paschen notation) to H($n=3$) as a function of the electron temperature. The cross sections for excitation of H($n=3$) and Ar($4p$) are taken from Refs. 45 and 46, respectively. A Maxwellian distribution for the EEDF was assumed.

III. THEORETICAL ANALYSIS OF ACTINOMETRY

A. Presentation of the method

Actinometry is a method which allows one to estimate relative concentrations and mole fractions of a ground electronic state species X from measurements provided by optical emission spectroscopy (OES). The principle of the method is based on the excitation processes of two species, the species X and the actinometer. In the case where:

(i) The actinometer does not perturb the plasma,
(ii) both species are excited to their respective radiative excited state by a direct electron impact process from their ground electronic state, and
(iii) the excitation process cross sections as a function of the electron energy have, for both species, the same shape and a similar threshold.
(iv) The quenching processes as well as all the other processes of loss of the excited state species are negligible,

Then, the reduced scheme for the excitation and deexcitation processes is the following:

$$X + e \rightarrow X^* + e$$

$$\mathrm{Act} + e \rightarrow \mathrm{Act}^* + e$$

$$X^* \rightarrow X + h\nu$$

$$\mathrm{Act}^* \rightarrow \mathrm{Act} + h\nu'$$

and there is a very simple relationship linking the emission intensity ratio to the concentration ratios of species X and actinometer

$$[X]/[\mathrm{Act}] = kI_X/I_{\mathrm{Act}}, \qquad (1')$$

where $[X]$ and $[\mathrm{Act}]$ are the concentrations of electronic ground state of X species and actinometer species, respectively, k a constant, and I_X/I_{Act}, the ratio of emission intensities of the excited X species and excited actinometer species. Very often, but not necessarily, a rare gas is chosen as an actinometer. Note that for X being identical to Act but emitting from a different electronic state, $I_X/I_{\mathrm{Act}} = k^{-1}$.

If the quenching processes as well as other processes leading to a loss of the excited state are not negligible, then the relationship is not linear. Also, if the excitation cross sections are not exactly proportional, the relationship is not linear. The constant k is a function of the electron energy distribution function (EEDF). For X equal to Act, k depends only on the EEDF and the quenching processes' (and other loss terms) efficiency.

B. Choice of actinometer for probing H atoms

Argon has been chosen as actinometer for studying the variations of the H-atom mole fraction under diamond deposition plasma conditions. It presents radiative states with excitation thresholds close to that of the H atom in the $n=3$ level: for instance, the $2p_1$ radiative state of argon has a threshold at 13.48 eV which is close to that of the H atom in the $n=3$ level (threshold 12.09 eV). The electron impact excitation cross sections of H($n=3$) and Ar($2p_1$) as functions of the electron energy can be found in Refs. 43–46. As the cross sections are not exactly proportional, the variations of the excitation rate constants ratio as a function of the EEDF [or the electron temperature (Te) if considering a Maxwellian distribution for the EEDF] must be taken into account. With the assumption of a Maxwellian EEDF, the variation of this ratio as a function of Te the range of 1000–30 000 K is given in Fig. 1. Although very sensitive to Te at low electron temperature, its variations are less important for Te ranging from 15 000 to 20 000 K. Under experimental conditions where the EEDF (and Te) present only slight evolution as a function of both the plasma parameters and the spatial coordinates, the choice of argon for probing the H atoms is expected to be reasonably good.

Other sublevels of Ar($4p$) such as the state $2p_9$, which has its excitation threshold at 13,05 eV, could also be *a priori* chosen, since the excitation threshold as well as the shape of the cross section are compatible with those of the excitation of H atoms to the $n=3$ level.

We now have to verify that all the excited species (Ar($4p$) (sublevels $2p_1$ and $2p_9$) and H($n=3$)) are mainly

TABLE I. Main processes of production and loss of $n=3$ excited state of hydrogen atom. From the balances of Tables I and II, the mole fractions of H($2s$) and H($n=3$) are approximately equal to 2.4×10^{-9} and 2.5×10^{-12} at Te=11 600 K, respectively, and to 1×10^{-8} and 4×10^{-9} at Te=23 000 K, respectively. The ground state H-atom mole fraction is assumed to be 4%.

Reactions	E_{thr} (eV)	σ_{MAX} (cm^2)	$\langle\sigma v\rangle$ at 1 eV (cm^3 s^{-1})	$\langle\sigma v\rangle$ at 2 eV (cm^3 s^{-1})	r (cm^{-3} s^{-1}) Te=11 600 K	r (cm^{-3} s^{-1}) Te=23 000 K	No.
Direct excitation $H(n=1)+e\rightarrow H(n=3(s,p,d))+e$	12.06	1.3×10^{-17} [a]	1.9×10^{-14}	4.8×10^{-12}	1.06×10^{14}	2.7×10^{16}	(1)
Excitation through metastable H($2s$) $H[n=2(s,p)]+e\rightarrow H(n=3(s,p,d))+e$	2	1×10^{-14} [b]	9.6×10^{-11}	2.4×10^{-10}	3.2×10^{10}	3.3×10^{11}	(2)
Dissociative excitation $H_2+e\rightarrow H(n=3)+H(n=1)+e$	19	2×10^{-18} [a]	2.7×10^{-17}	1.8×10^{-13}	3.85×10^{12}	2.5×10^{16}	(3)
Radiative de-excitation $H(n=3(s,p,d))\rightarrow H[n=2(s,p)]+h\nu$		Aij (s^{-1}) $=4.36\times10^{7}$ [c]			1.08×10^{13}	0.9×10^{16}	(4)
Radiative de-excitation $H(3p)\rightarrow H(1s)+h\nu$		Aij (s^{-1}) $=5.39\times10^{7}$ [c]			2.4×10^{13}	1.2×10^{16}	(5)
Quenching by H_2 molecules $H(n=3)+H_2\rightarrow H(n=1)+H_2$		60×10^{-16} [d]	3×10^{-9}	3×10^{-9}	7.5×10^{13}	3.6×10^{16}	(6)
Quenching by H atoms $H(n=3)+H\rightarrow H(n=1)+H$		[e]			Weak unless x_H high	Weak unless x_H high	(7)
Ionization: $H(n=3)+e\rightarrow H^+ +e+e$	1	$<6\times10^{-15}$ at 1 eV [b]	4×10^{-7}	1.4×10^{-10}	1.4×10^{11}	1.7×10^{15}	(8)

[a]References 43 and 44.
[b]Reference 45.
[c]References 45 and 70.
[d]References 29 and 27.
[e]This work.

excited from their corresponding electronic ground states through a direct electron impact. Calculations based on kinetics[43–73] allow us to estimate the relative importance of the different mechanisms in the production of the argon and hydrogen atoms in their excited states.

C. Excitation and loss processes of H($n=3$) and Ar($4p$) in the plasma

The processes involved for the production and the consumption of the H($n=3$) electronic state of H atom are given on Table I. Rates of the processes calculated assuming a Maxwellian distribution for the electron energy and electron temperatures of 11 600 and 23 000 K, respectively, are also given in Table I. The references from which the cross sections have been taken are given in the table. These data allow us to estimate the processes which can be neglected, and those which are predominant, as a function of the electron temperature assuming a H-atom mole fraction of 4%. Since H($n=2$) may be an intermediate step for the excitation of H($n=3$), its production and loss terms have been analyzed. The reactions as well as their rates at 11 000 and 20 000 K for Te are given on Table II. The main processes for the production and the destruction of the $4p$ excited electronic Ar atom are presented in Table III.

In principle, actinometry can be used only if the excitation processes (1) and (24) or (25), and de-excitation processes (4) and (29) or (30) are predominant. However, owing to the high pressure characterizing diamond deposition reactors, nonradiative processes such as quenching processes [reactions (6), (19), and (33)] are seen to be efficient in depopulating the excited states leading to a loss in the emission intensities. These processes, the importance of which depends on pressure and gas temperature, must then be taken into account.

1. Production and loss terms for Ar($4p$)

At pressure as high as those used for growing diamond under microwave plasma (2000–10 000 Pa), quenching rates of metastable argon-atom [reactions (32) and (33)] are high versus the rates of excitation to the upper excited state [reactions (28) and (29)] (Table III). This prohibits the role of metastables from producing argon $4p$ excited states, as well as producing H atoms in the $n=2$ level [reactions (11) and (12)]. We can conclude then that excited $4p$ level of argon is mainly produced through direct electron impact.

We have measured the emission intensity of lines corresponding to two transitions of sublevels of the Ar($4p$) state as a function of the percentage of argon introduced (0%–4%) (Fig. 2). Sublevel $2p_1$, with an excitation threshold 13.48 eV, de-excites on the radiative state $1s_2$ [reaction (30)], while sublevel $2p_9$, with an excitation threshold 13.05 eV, de-excites on the metastable state $1s_5$ [reaction (31)]. As, for both lines, the emission intensities $I_{750,3}$ [reaction (30)] and $I_{811,5}$ [reaction (31)] are proportional to the amount of argon introduced (up to 4%), we can conclude that the self-absorption of the 811.5 nm line, which could occur efficiently since state $1s_5$ is metastable, is negligible. Thus, owing to the high efficiency of the quenching, metastables of argon do not participate to the production of $2p_9$ sublevel, under the conditions used here. Nevertheless, in order to maintain the role of metastables as low as possible, for the whole study, the percentage of argon has been limited to 1 vol %.

Therefore, both states $2p_1$ and $2p_9$ can be used for performing actinometry under diamond deposition conditions. The ratio of emission intensities issued from these two sublevels is directly related to the proportionality factor $k(Te,k_Q)$ which depends on Te and quenching terms. As we have verified that the quenching cross sections are identical

TABLE II. Main processes of production and loss of metastable $2s$ excited state of hydrogen atom. From the balances of Tables I, II, and III, the mole fractions H($2s$), H($n=3$) and Ar($^3P_2$) are approximately equal to 2.4×10^{-9}, 2.5×10^{-12}, and 1.4×10^{-11} respectively, at Te=11 600 K and to 1×10^{-8}, 4×10^{-9}, and 2.7×10^{-9}, respectively, at Te=23 000 K.

Reactions	E_{thr} (eV)	σ_{MAX} (cm^2)	$\langle\sigma v\rangle$ at 1 eV (cm^3 s^{-1})	$\langle\sigma v\rangle$ (cm^3 s^{-1}) at 2 eV	r (cm^{-3} s^{-1}) Te=11 600 K	r (cm^{-3} s^{-1}) T_e=23 000 K	No.
Direct excitation							
$e+H(n=1)\rightarrow e+H(2s)$	10.2	1×10^{-17} [a]	1.09×10^{-13}	1.14×10^{-11}	6.13×10^{14}	6.4×10^{16}	(9)
$e+H(n=2s)\rightarrow e+H(2p)$	1.9	10^{-13} [b]	5×10^{-6}	5×10^{-6}	1.68×10^{15}	7×10^{15}	(10)
$H[n=2(s,p)]+e\rightarrow H(n=3(s,p,d)+e$	2	1×10^{-14} [b]	9.6×10^{-11}	2.4×10^{-10}	3.2×10^{10}	3.3×10^{11}	(2)
Excitation through metastable of argon							
$Ar(^3P_0)+H(n=1)\rightarrow H[n=2(s,p)]+Ar(^1S_0)$		0.9×10^{-16} [c]	8×10^{-11}	7×10^{-11}	$<5\times10^{12}$	$<5\times10^{13}$	(11)
$Ar(^3P_2)+H(n=1)\rightarrow H[n=2(s,p)]+Ar$		10×10^{-16} [d]	8×10^{-10}	7×10^{-10}	4×10^{13}	5×10^{14}	(12)
Dissociative excitation	23	3×10^{-18} [b]	5.6×10^{-19}	2.4×10^{-14}	7.84×10^{10}	3.4×10^{15}	(13)
$H_2+e\rightarrow H(n=2s)+H(n=2p)+e$							
Dissociative excitation	14.9	1.5×10^{-17} [b]	1.38×10^{-15}	1.2×10^{-12}	1.93×10^{14}	1.7×10^{17}	(14)
$H_2+e\rightarrow H(n=2s)+H(n=1)+e$		1.5×10^{-16} (at 1 eV)					
$e+H_3^+\rightarrow H_2(v>5)+H(n=2)$		6×10^{-16} [b]	4×10^{-8}	3×10^{-8}	6×10^{16}	4.5×10^{16}	(15)
$e+H(n=2s)\rightarrow e+H^++e$	3.4	8×10^{-16}	3.43×10^{-11}	1.5×10^{-10}	1.15×10^{10}	2.1×10^{11}	(16)
Mixing by electric field: $H(2s)\rightarrow H(2p)$		e			1.68×10^{-15}	1×10^{16}	(17)
Radiative de-excitation		Aij (s^{-1})			9×10^{16}	3×10^{17}	(18)
$H(2p)\rightarrow H(1s)+h\nu$		$=6.27\times10^{8}$ [b]					
Quenching		50×10^{-16} [f]	2.5×10^{-9}	2.5×10^{-9}	5×10^{16}	2.5×10^{17}	(19)
$H(2s)+H_2\rightarrow H_3^++e$							
Collisional mixing		80×10^{-16} [g]	4×10^{-9}	4×10^{-9}	8×10^{16}	4×10^{17}	(20)
$H(2s)+H_2\rightarrow H(2p)+H_2$							
Dissociative quenching		Weak versus (18)[h]					(21)
$H(2s)+H_2\rightarrow H(1s)+H(1s)+H(1s)$							
Collisional mixing		$100-200\times10^{-16}$ [i]	$<1.4\times10^{-10}$	$<1.4\times10^{-10}$	2.8×10^{13}	1.4×10^{14}	(22)
$H(2s)+Ar\rightarrow H(2p)+Ar$							
Quenching		Same magn as			Same magn as	Same magn as	(23)
$H(2p)+H_2\rightarrow$product		(19)			(19)	(19)	

[a]References 43 and 44.
[b]Reference 45.
[c]References 47, 48, 71, and 78.
[d]Reference 48.
[e]References 49 and 52.
[f]Reference 52.
[g]References 53–56.
[h]Reference 57.
[i]References 53–55, 57, and 58.

for these two sublevels (see later), k mainly depends on Te. As variations in the electron temperature induce variations in the ratio of excitation rate constants of the two excited states (Fig. 3), the emission intensity ratio of these lines might be used for getting information concerning the tendencies of variations of Te, as the function of the operating conditions (see Sec. VI B).

2. Production and loss terms for H($n=3$)

a. Processes involving ions and radiative cascades. H($n=3$) may be produced from reactions (1), (2), and (3). In addition, ion collisional reactions and radiative cascades (not given in the table) may contribute to the production of H($n=3$).

Ions: We have neglected most of the ion collisional reactions owing to the small populations of ions according to calculations. For conditions where power density is maintained at 9 W cm^{-3} (corresponding to Te close to 20 000 K at the plasma/surface interface), the calculated magnitudes for mole fractions of the main ions[17,74] are 10^{-5}, 5×10^{-7}, 5×10^{-9}, and 5×10^{-9} for H_3^+, H^+, H_2^+ and H^-, respectively, while the electron mole fraction is estimated at around 10^{-5}. With these values and the rate constants given by Janev *et al.*,[45] we can show that the only reaction involving ions which may participate indirectly to the production of H($n=3$) is reaction (15), since it produces H($n=2$). However, as shown in Table I and later in the text, the final participation of H($n=2$) to production of H($n=3$) [reaction (2)] is negligible versus reaction (1). The process leading directly to the production of H($n=3$) by dissociative recombination of H_2^+ is thus inefficient under our conditions. This is confirmed experimentally by the fact that it would produce H($n=3$) atoms with high translational energy which were not observed.[32,85]

Radiative cascades: As the population and the spontaneous emission coefficient of the excited states decrease as a function of the principal quantum number,[75,76] we can assume that the production of the H($n=3$) species through radiative cascades, if efficient, would only involve the H($n=4$) excited level. Gordon *et al.*[74,75] have measured a value of 10^{-12} for the H($n=4$)-atom mole fraction, under typical conditions corresponding to diamond deposition microwave

TABLE III. Main processes of production and loss of some excited states of argon atom. From reactions (27) and (12), at Te=11 600 K, the Ar ($^3P_2$) mole fraction is estimated at 1.4×10^{-11}, that of Ar($^3P_0$) should be less by a factor 5–7 (Ref. 47). Mole fraction of Ar[$4s(2p_9)$] level is estimated at around 1.4×10^{-13}, that of Ar[$4s(2p_1)$] at 2.25×10^{-13}.

Reactions	E_{thr} (eV)	σ_{MAX} (cm^2) or Aij (s^{-1})	$\langle\sigma v\rangle$ at 1 eV (cm^3 s^{-1})	$\langle\sigma v\rangle$ at 2 eV (cm^3 s^{-1})	r (cm^{-3} s^{-1}) Te=11 600 K	(cm^{-3} s^{-1}) Te=23 000 K	No.
Direct excitation	13.48	11×10^{-18} [a]	5.3×10^{-15}	2.52×10^{-12}	7.4×10^{12}	3.5×10^{15}	(24)
Ar(3p)+e→Ar[4p($^2p_1$)]+e							
Direct excitation	13.05	22×10^{-18} [b]	3.26×10^{-15}	7.31×10^{-13}	4.6×10^{12}	10^{15}	
Ar(3p)+e→Ar[4p($^2p_9$)]+e							(25)
Excitation to metastable		Around	2.7×10^{-14}	5.8×10^{-12}			
Ar(3p)+e→Ar($^3P_0$)+e	11.72	0.6×10^{-16} [c]			$<4\times10^{13}$	$<8\times10^{15}$	(26)
Ar(3p)+e→Ar($^3P_2$) (state $1s_5$)+e	11.54	0.6×10^{-16} [c]	3.2×10^{-14}	6.2×10^{-12}	4.5×10^{13}	8.4×10^{15}	(27)
Excitation through metastable	1.46	Upper value	Max: 2×10^{-7}	Max 2.4×10^{-6}	$\ll4\times10^{11}$	$\ll5.5\times10^{14}$	(28)
Ar($^3P_0$)+e→Ar[4p($^2p_1$)]+e		80×10^{-16} [d]	more probable 10^{-8}	2.5×10^{-8}	More probable $<2\times10^{10}$	More probable $<10^{13}$	
Ar($^3P_2$)+e→Ar[4p($^2p_9$)]+e	1.51	Idem[d] as (28)	Idem as (28)	Idem as (28)	Max 4×10^{11} 2×10^{10}	Max 5.5×10^{14} 10^{13}	(29)
Radiative de-excitation on radiative state		Aij (s^{-1})			Around	8×10^{14}	(30)
Ar[4p($^2p_1$)]→Ar[4s($^1s_2$)]+hν		$=4.72\times10^{7}$ [e]			7×10^{11}		
Radiative de-excitation on $^3P_2$ metastable state		Aij			Around	10^{14}	(31)
Ar[4p($^2p_9$)]→Ar[4s($^1s_5$)]+hν		$=3.66\times10^{7}$ [e]			6×10^{11}		
Metastable quenching							
Ar(4s($^3P_0$,$^3P_2$)+(H)→Ar(3p)+H($n=2$)		10×10^{-16} [f]	8×10^{-10}	7×10^{-10}	4×10^{13}	5×10^{14}	(11),(12)
Ar(4s)+(H_2)→Ar[3p($^1S_0$)]+H_2($a^3\Sigma_g^+$)		4×10^{-16} [g]	2.8×10^{-10}	2.8×10^{-10}	4×10^{13}	7.6×10^{15}	(32)
Leading to H(1s)+H(1s)							
Quenching of 4p state		$40-70\times10^{-16}$ [h]	2.8×10^{-9}	2.8×10^{-9}	$4-7\times10^{12}$	$1-3\times10^{15}$	(33)
Ar(4p)+(H_2)→Ar(product)+H_2							

[a]References 46, 63, and 64.
[b]Reference 46.
[c]References 65 and 67.
[d]References 68 and 69.
[e]Reference 70.
[f]Reference 48.
[g]References 71 and 73.
[h]This work.

discharges. The estimated contribution of H($n=4$) to the production of H($n=3$) is around 1000 times less than the production through a direct electron impact from the electronic ground state [reaction (1)]. Also, the radiative decay of H($n=3$), the mole fraction of which varies from 10^{-12} at 11 000 K to 10^{-9} at 20 000 K, towards H($n=2$) is inefficient for producing H($n=2$).

The low populations of electronic excited states are attributed to the high quenching efficiency (high pressure) and to the relatively low electron temperature under these condi-

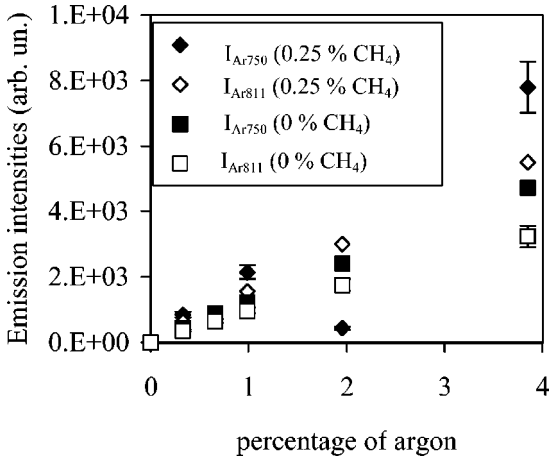

FIG. 2. Variations of emission intensities of lines issued from Ar($4p$) ($2p_1$ state and $2p_9$ states) as a function of the percentage of argon introduced in the feed gas, and for two percentages of methane introduced in the feed gas (0% CH_4 and 0,2% CH_4). Discharge conditions: pressure: 2500 Pa, microwave power: 600 W.

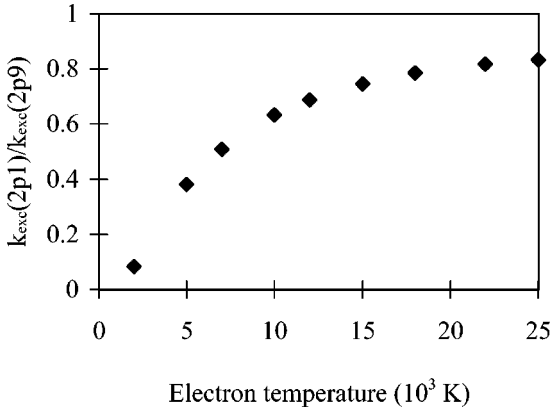

FIG. 3. Variations of the ratio of electron excitation rate constants of Ar($4p$) ($2p1$ state) to Ar($4p$) ($2p_9$ state) as a function of the electron temperature. The excitation cross sections are taken from Ref. 46. A Maxwellian distribution for the EEDF was assumed.

tions. We can also assert that the contribution of radiative decay processes to the population of a given level is decreasing as the pressure increases, since the electron temperature simultaneously decreases[17] while the quenching efficiency increases.

b. Contribution of metastable $H(2s)$ atom to the production of $H(n=3)$. The rate for the mechanism of production of H(3) involving the $H(2s)$ state (nonradiative state) [reaction (2)], depends on the rate constant of the process as well as on the $H(2s)$ and on the electron densities. The rate must be compared to the rate of the direct electron excitation mechanism [reaction (1)]. The density of the $H(2s)$ depends on its production and on its consumption rates.

The observation of Table II shows that the main processes leading to the production of metastable $H(2s)$ state are reactions (9), (14), and (15). The contribution of metastable argon to the production of $H(n=2)$ is seen to be negligible. The $H(n=2s)$ consumption is due on the one hand to nonradiative quenching processes [reactions (19)][52] which occur with high collisional frequency ($\nu_Q = 3{,}4\times10^8$ s^{-1}, at 2500 Pa and 2200 K). On the other hand, the mixing with $H(2p)$ state followed by its radiative decay [reaction (18) which occurs with an Einstein coefficient of $4{,}7\times10^8$ s^{-1}], can be very efficient in reducing the lifetime of $H(2s)$. The mixing processes are due to the action of the electric field[49–52] [reaction (17)] and to the collisional mixing during collisions with H_2 molecules [reaction (20)].[52–56] These occur with high collisional frequencies, estimated at $\nu_{ME} \cong 7\times10^6$ s^{-1}, and $\nu_{MQ} \cong 4{,}8\times10^8$ s^{-1}, respectively, under microwave plasma diamond deposition conditions. At high pressure, trapping processes (self-absorption) might contribute to maintain a relatively high population of $H(2p)$ [and then $H(2s)$].[59–61] Under diamond deposition conditions, the escape factor due to trapping processes has been estimated, and the radiative lifetime of $H(2p)$ was seen to increase from 2×10^{-9} s (lifetime for isolated species) to 125×10^{-9} s, due to trapping. However, under these conditions, the main channel for destruction of the $H(2s)$ state [as well as $H(2p)$] is through the nonradiative quenching processes [reaction (19)]. The corresponding lifetime for the $H(2s)$ and $H(2p)$ states was finally estimated at 3×10^{-9} s.

Finally, for electron temperatures of 11 600 and 23 000 K, the density of $H(2s)$ is estimated at 2×10^8 and 10^9 cm^{-3}, respectively. For a H-atom mole fraction of 4%, the ratio of the rate of reaction (1) over that of reaction (2) varies from 3×10^3–10^5 as the electron temperature increases from 11 000 to 20 000 K. Channel (2) is then negligible relative to channel (1) for producing $H(n=3)$, under these deposition conditions.

C. Contribution of the dissociative excitation reaction to the production of $H(n=3)$. For a H-atom mole fraction of 4%, as shown on Table I, although negligible at Te equal 11 000 K, the dissociative excitation mechanism [reaction (3)] competes with channel (1) for the production of $H(3s)$ for Te equal 23 000 K. This should prohibit the use of actinometry under such conditions.[62,77]

The ratio R of rates of production of $H(n=3)$ from channel (1) and channel (3) can be estimated systematically as a function of the electron temperature and the H-atom mole fraction, assuming or not a Maxwellian distribution for the EEDF. Assuming a Maxwellian distribution for the EEDF, the variations of $R = k_e^{H\alpha} n_H / k_{diss} n_{H2}$ as a function of Te (from 1 to 2 eV) and for different H-atom mole fractions are presented in Fig. 4. The terms $k_e^{H\alpha}$ and k_{diss} are the rate constants, respectively, of reactions (1) and (3), and, n_H and n_e, respectively, the electron and H-atom densities. A strong dependance of R vs Te and H-atom mole fraction is observed. At electron temperatures higher than 20 000 K associated to a H-atom mole fraction of 3%–5%, the validity of actinometry is seen to be critical since the dissociative excitation process [reaction (3)] becomes competitive with the direct electron impact excitation process [reaction (1)]. For lower electron temperature, the corresponding H-atom mole fraction at which the dissociative excitation process contribution is negligible is lowered (Fig. 4). When assuming a non-Maxwellian distribution,[76] the boundary condition is slightly shifted to higher electron temperature since Maxwellian distribution overestimates processes with energy threshold more than 12 eV and underestimates processes with energy less than 12 eV.

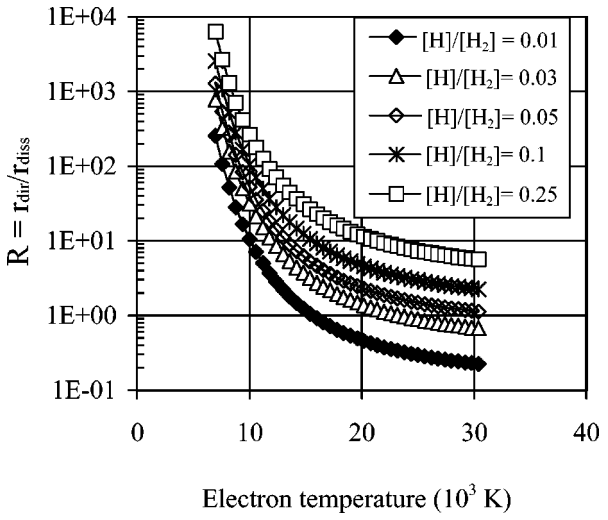

FIG. 4. Variations of the direct excitation process rate to the dissociative excitation process rate leading to the production of $H(n=3)$ as a function of the electron temperature and different H-atom mole fractions. A Maxwellian distribution for the EEDF was assumed.

Calculations realized with a 1D diffusive H_2 plasma flow model[17] indicated that the experimental conditions leading to an electron temperature of 20 000 K and a H-atom mole fraction of 3%–5% correspond to a power density of around 9 W/cm^3, obtained with a power of 600 W and a pressure of 2500 Pa. These specific experimental conditions should constitute the lower boundary conditions in terms of power density (lowest power and pressure) for which actinometry is valid. We will compare later (Sec. VI B) actinometry and TALIF when these lower boundary conditions are used and conclude or not on the validity of actinometry for these conditions (9 W cm^{-3}). Later on, we will also work on finding an upper boundary condition in terms of power density which may limit the use of actinometry at very high power densities (Sec. VI C).

D. Relation linking H-atom mole fraction to emission intensities (OES)

Under the conditions tested here, owing to the high pressure (>500 Pa), we can consider that ionization (and excitation) processes [reaction (8)] are negligible compared to the quenching processes [reaction (6)]. Also, ionization of $Ar(4p)$ is negligible versus quenching reactions [reactions (32) and (33)]. The proportionality constant k linking the ground state H atoms' concentration to the ratio $I_{H\alpha}/I_{Ar}$ not only depends on the electron temperature [variation of the excitation rate constants ratio (Fig. 2)], but also on the collisional quenching terms. These latter processes concern mainly the quenching processes of $H(n=3)$ and $Ar4p'[1/2]$ by ground state H_2 molecules and H atoms, which are the main species in the plasma.[17,76] Then

$$\frac{[H]}{[Ar]}=\frac{x_H}{x_{Ar}}=k(\text{EEDF, quenching terms})\,\frac{I_{H\alpha}}{I_{Ar}}=\frac{k_e^{Ar^*}}{k_e^{H\alpha}}\left[\frac{\nu_{Ar^*}}{\nu_{H\alpha}}\right]Q_T\,\frac{I_{H\alpha}}{I_{Ar}}\,F, \tag{2'}$$

where $k_e^{Ar^*}$ and $k_e^{H\alpha}$ are the excitation rate constants[43,44,46] for the transitions $Ar(3p)\rightarrow Ar(4p)$ and $H(n=1)\rightarrow H(n=3)$, respectively, ν_{Ar^*} and $\nu_{H\alpha}$ the de-excitation frequencies for H_α and Ar* transitions, and x_H and x_{Ar}, respectively, the H-atom and Ar-atom mole fractions. Q_T is the de-excitation term taking into account all the processes of radiative de-excitation and collisional quenching. F is an optical device factor.

Since $H(n=3)$ is mainly populated by collisions between electron and ground state H atoms, the $H(n=3)$ sub-distribution on the $3s$, $3p$, and $3d$ excited states sublevels is assumed to be the statistical weighting given by the number of sublevel degeneracies of each angular momentum L state. Then, the sub-distribution of the $n=3$ level is 11.8%, 33.3%, and 55.5%, respectively, for the $3s$, $3p$, and $3d$ states.[29] The emission intensity of H_α is equal to

$$I_{H\alpha}=K(\nu_{H\alpha})A_{32}\nu_{H\alpha}v_{\text{emiss.}}\,\frac{[H(n=1)]k_e^{H\alpha}n_e+k_{\text{diss}}[H_2]n_e}{[H]k_{QH\alpha/H}+[H_2]k_{QH\alpha/H2}+k_R}, \tag{3'}$$

where A_{ij} (i and j refer to upper and lower electronic states) are obtained from the Einstein coefficients for the spontaneous radiative de-excitations, $k_R=(A_{32}+A_{31})$, and $A_{32}=([3s]/\tau_s)+([3p]^*f_p/\tau_p)+([3d]/\tau_d)$, where τ_s, τ_p, and τ_d are, respectively, the lifetimes of the $3s$, $3p$, and $3d$ levels. The term f_p represents the branching term of de-excitation of the $3p$ level towards the $2s$ level relative to the $1s$ level. $A_{32}=(0{,}118/159\times10^{-7})+(0{,}333^*0{,}1183/5{,}4\times10^{-7})+(0{,}555/15{,}6\times10^{-7})=4{,}36\times10^7\ s^{-1}$ and $A_{31}=[3p]^*(1-f_p)/\tau_p)=5{,}39\times10^7\ s^{-1}$ which leads to a total radiative de-excitation rate constant $k_R=A_{32}+A_{31}=9{,}8\times10^7\ s^{-1}$.

$K(\nu_{H\alpha})$ is a constant taking into account the optical device response, $k_{QH\alpha/H2}$ and $k_{QH\alpha/H}$ represent the quenching rate constants of H_α by the H_2 molecules and the H atoms, respectively, and are equal to $v_{H/H_2}\sigma_{H\alpha/H2}$ and $v_{H/H}\sigma_{H\alpha/H}$. The terms v_{H/H_2} and $v_{H/H}$ are the respective relative mean velocities of H_α atom and H_2 molecules and H_α and H atoms and $\sigma_{H\alpha/H_2}$ and $\sigma_{H\alpha/H}$ the quenching cross sections of H_α by the H_2 molecules and by the H atoms.

Neglecting the dissociative excitation mechanism [reaction (3)] leads to

$$I_{H\alpha}=(K(\nu_{H\alpha})\nu_{H\alpha}A_{32}v_{\text{emss.}}/k_R)\times\frac{\{[H(n=1)]k_e^{H\alpha}n_e\}}{\{[H](k_{QH\alpha/H}/k_R)+[H_2](k_{QH\alpha/H_2}/k_R)+1\}}. \tag{4'}$$

Concerning the excitation of argon, we have

$$I_{Ar}=K(\nu_{Ar^*})\nu_{Ar^*}A_{44}v_{\text{emss.}}\times\frac{[Ar(3p)]k_e^{Ar^*}n_e}{[H]k_{QAr^*/H}+[H_2]k_{QAr^*/H_2}+k_{RAr}}, \tag{5'}$$

where A_{44} is the Einstein coefficient for the spontaneous transition $Ar(4p)\rightarrow Ar(4s)$ ($k_{RAr}=A_{44}$), k_{QAr^*/H_2} and $k_{QAr^*/H}$ are the quenching terms of Ar* by molecular hydrogen and atomic hydrogen. The terms $k_{QAr^*/H_2}=v_{Ar/H_2}\sigma_{Ar^*/H_2}$ and $k_{QAr^*/H}=v_{Ar/H}\sigma_{Ar^*/H}$, where v_{Ar/H_2} and $v_{Ar/H}$ are the relative mean velocities between Ar and H_2 and H, respectively, and σ_{Ar^*/H_2} and $\sigma_{Ar^*/H}$ the associated quenching cross sections. $K(\nu_{Ar^*})$ is a constant taking into account for the optical device response.

Finally

$$\frac{[H(n=1)]}{[Ar(3p)]}=\frac{x_H}{x_{Ar}}=F\,\frac{k_e^{Ar^*}}{k_e^{H\alpha}}\,Q_T I_{H\alpha}/I_{Ar} \tag{6'}$$

with

$$F=\frac{K(\nu_{Ar^*})(\nu_{Ar^*}A_{44}/k_{RAr})}{K(\nu_{H\alpha})[\nu_{H\alpha}A_{32}/(A_{32}+A_{31})]} \tag{7'}$$

and

$$Q_T=\frac{1+(P/RT(A_{32}+A_{31}))[v_{H/H_2}\sigma_{H\alpha/H_2}x_{H_2}+v_{H/H}\sigma_{H\alpha/H}(1-x_{H_2})]}{1+(P/RTA_{44})[v_{Ar/H_2}\sigma_{Ar^*/H_2}x_{H_2}+v_{Ar/H}\sigma_{Ar^*/H}(1-x_{H_2})]}. \tag{8'}$$

Q_T is a factor which represents the effect of all quenching

$$Q_T=\frac{\{1+PT^{-1/2}[0{,}132\sigma_{H\alpha/H_2}x_{H_2}+0{,}152\sigma_{H\alpha/H}(1-x_{H_2})]\}}{\{1+PT^{-1/2}[0{,}162\sigma_{Ar*/H_2}x_{H_2}+0{,}226\sigma_{Ar*H}(1-x_{H_2})]\}}. \quad (9')$$

Note that the quenching of H_α by argon atoms has been neglected due to the small amount of argon introduced and to the small cross section of the process ($\sigma_{H\alpha/Ar}/\sigma_{H\alpha/H_2}=0.3$).[27,29] Also, the quenching of Ar* by Ar atoms has been neglected since it is very small ($\sigma_{Ar*/Ar}/\sigma_{H\alpha/H_2}=0.027$).

Under conditions of low dissociation yield of molecular hydrogen, the contribution of the quenching by H atoms can be neglected, and Q_T replaced by Q_{H_2}. Q_{H_2} takes into account the effect of quenching processes by molecular hydrogen relative to radiative de-excitation.

$$\text{with } Q_{H_2}=\frac{[1+0.132x_{H_2}\sigma_{H\alpha/H_2}PT^{-1/2}]}{[1+0.162x_{H_2}\sigma_{Ar*/H_2}PT^{-1/2}]}. \quad (10')$$

Relationship (6′) linking the H-atom mole fraction to the Ar-atom mole fraction and the emission intensities ratio $I_{H\alpha}/I_{Ar}$ is valid only if actinometry is valid.

IV. EXCITATION PROCESSES BY TWO PHOTON ALLOWED TRANSITION LIF (TALIF)

H-atom concentration is here proportional to the product of the fluorescence amplitude by its width $\Delta\lambda_D$, (that is to the area), and to a factor taking into account the quenching due to the collisional de-excitation of the H atoms before they fluoresce. However, absolute values of concentrations can only be reached after calibration which can be made, for instance, by titration or absorption techniques.[62]

The additional processes of excitation and de-excitation of the H($n=3$) excited state of H atom, which must be considered in this new configuration, are the following:

$$\text{Laser excitation: } H(n=1)+2h\nu\rightarrow H(n=3s,3d), \quad (34)$$

$$\text{Collisional mixing: } H(n=3s,d)+M_i\rightarrow H(n=3s,p,d), \quad (35)$$

$$\text{Three photon ionization process: } H(n=3)+h\nu\rightarrow H^+. \quad (36)$$

H($n=3$) atoms are produced by two direct mechanisms: laser excitation [reaction (34)] and electron impact excitation [reaction (1)], however we can assume[78] that the excitation by the laser is more powerful than that by the electrons. In addition, the three photon ionization [reaction (36)] is negligible compared to the quenching of the H($n=3$) atoms [reactions (6) and (7)]. The fluorescence signal area including all the radiative processes leading to the H($n=3$) level is then given by

$$(I_{H\alpha})_{fluo}=\frac{K'(\nu_{H\alpha})v_{emiss.}A'_{32}\nu_{H\alpha}W_{13}^2/k_R}{1+k_Q[M]/k_R}[H(n=1)], \quad (11')$$

where

$$k_Q[M]=(P/RT)[v_{H/H_2}\sigma_{H\alpha/H_2}x_{H_2}+v_{H/H}\sigma_{H\alpha/H}(1-x_{H_2})]$$

and $k_R=A'_{32}+A'_{31}$ where $A'_{32}+A'_{31}$ are calculated from the Einstein coefficients for the spontaneous emissions {H[$n=3(s,p,d)$]$\rightarrow$H($n=2s,p,1s$)}.[29] W_{13} is the two photon excitation rate coefficient, v_{emiss}. the emissive volume, and $K'(\nu_{H\alpha})$ an optical device factor.

As the main process for production is laser excitation, H($n=3$) sub-distribution is not given by the statistical distribution as it is the case when electron excitation is predominant. The distribution depends on the electric field polarization of the laser light in the direction of propagation which interacts with the medium. In our case, the distribution is the same as that reported by Preppernau *et al.*[29] and Tung *et al.*:[79] 12% of $3s$ state and 88% of $3d$ state. However, according to Preppernau *et al.*, an almost total mixing is attained for lifetimes larger than 1 ns.[29] As a consequence, for conditions where the H($n=3$) lifetime is more than 1 ns, the statistical distribution between $3s$, $3p$, and $3d$ states is reached whether the excitation is due to laser or to electron impact. This is the case for the operating conditions reported here where lifetimes of H($n=3$) varying from 1 to 2.5 ns have been estimated.

In a pure hydrogen plasma, under conditions where the H($n=3$) lifetime is larger than 1 ns, the quenching contribution with respect to radiation is then given by

$$k_Q[M]/k_R=(0.132x_{H_2}\sigma_{H\alpha/H_2}+0.152x_H\sigma_{H\alpha/H})PT^{-1/2}, \quad (12')$$

where P is given in hPa (10^2 Pa), T in K, and the cross sections in Å^2. Then

$$x_H=\frac{RT(I_H)_{fluo}\{[PT^{-1/2}(0.132x_{H_2}\sigma_{H\alpha/H_2}+0.152x_H\sigma_{H\alpha/H})]+1\}}{PK'(\nu_{H\alpha})\nu_{H\alpha}v_{emiss.}W_{13}^2}. \quad (13')$$

At low dissociation yield

$$x_H=(I_{H\alpha}T/P)_{fluo}\{B/W_{13}^2\}\times[1+0.132x_{H_2}\sigma_{H\alpha/H_2}PT^{-1/2}], \quad (14')$$

with $B=R/[\nu_{H\alpha}v_{emiss.}K'(\nu_{H\alpha})]$

V. ESTIMATION OF THE QUENCHING CROSS SECTIONS

The four quenching cross sections ($\sigma_{H\alpha/H_2}$, σ_{Ar*/H_2}, $\sigma_{H\alpha/H}$, σ_{Ar*/H_2}) are needed for estimating the relative variations of the H-atom mole fraction as a function of the plasma parameters. The only cross section determined experimen-

tally with a good accuracy is $\sigma_{H\alpha/H_2}$. Bittner *et al.*[27] and Preppernau *et al.*[29] reported values of 65 and 58 Å^2, respectively. The terms σ_{Ar^*/H_2} has been estimated experimentally by us as explained below, while the other cross sections are calculated on the hard sphere model basis. However, the lack of knowledge of the collisional diameter for excited states leads obviously to some uncertainties on the variation of Q_T as a function of the plasma parameters.

A. Estimation of the quenching cross section of Ar($4p$) by H_2 molecules (σ_{Ar^*/H_2})

For estimating σ_{Ar^*/H_2}, experiments were carried out under low H-atom mole fraction (low dissociation yield) in order to minimize the contribution of the quenching of Ar($4p$) by H atoms (unknown). In addition, the conditions were chosen in such a way that the lifetime of H($n=3$) is high enough that we can consider that the statistical distribution is attained even when laser excitation is predominant [H($n=3$) lifetime larger than 1 ns].

At low H-atom mole fraction, a very simple relationship linking the actinometric signal $(I_{H\alpha}/I_{Ar})$ to that of TALIF $(I_{H\alpha})_{fluo}$ is derived from relations (6′), (10′), and (14′)

$$\frac{(I_{H\alpha}/I_{Ar})_{act}}{(I_{H\alpha}T/P)_{fluo}} = \frac{A}{x_{Ar}}[1+0.162\sigma_{Ar^*/H_2}x_{H_2}PT^{-1/2}], \quad (15')$$

$$\text{with } A=A(\text{EEDF},W_{13}^2)=\frac{\dfrac{Bk_e^{H\alpha}}{(k_e^{Ar^*}W_{13}^2)}}{F}. \quad (16')$$

Experiments were carried out in a region of the plasma where dissociation is still low. At the entry boundary of the plasma (edge of the plasma), the residence time of the species is low as well as the microwave energy deposited in the plasma (see later). In this region, gas temperature, $I_{H\alpha}/I_{Ar}$ (the 750 nm line was used for argon) and fluorescence signal were measured as a function of microwave power and pressure. The variations of $I_{H\alpha}/I_{Ar}$ and the fluorescence signal were measured. The variations of $I_{H\alpha}/I_{Ar}$ and of the fluorescence signal were seen to be small indicating that the dissociation remained low. Under these conditions, we have considered that x_{H_2} and x_{Ar} are constant at 1 and 0.01, respectively. The term $k_e^{H\alpha}/k_e^{Ar^*}$ was also considered as constant.

The plot of $(I_{H\alpha}/I_{Ar})_{act}/(I_{H\alpha}T/P)_{fluo}$ as a function of $PT^{-1/2}$ is presented in Fig. 5. A straight line is obtained indicating that the assumptions made previously are quite reasonable for the domain of pressure and temperature considered. In particular, the dissociative excitation process does not appear to be important under the conditions considered here, otherwise a straight line would not be found. From the slopes and origins, an estimate of the cross section for the quenching of Ar($4p$) by molecular hydrogen is obtained. The linear regression provides a value of 65 Å^2. However, owing to the assumptions made, a rather large error on the value given for σ_{Ar^*/H_2} is expected. A value of 65 Å^2 constitutes then a magnitude for σ_{Ar^*/H_2}, which is consistent with our experiments.

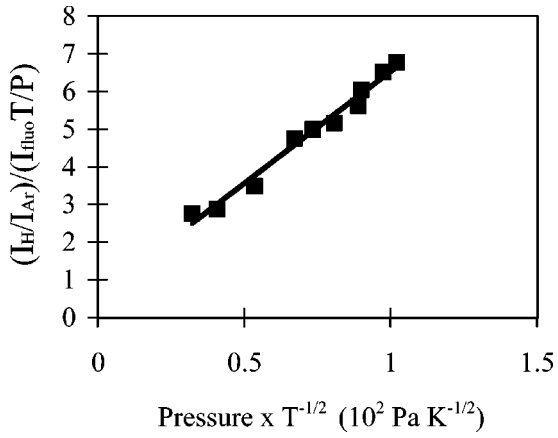

FIG. 5. Plot of $(I_{H\alpha}/I_{Ar})_{act}/(I_{H\alpha}T/P)_{fluo}$ vs $PT^{-1/2}$. The slope and origin of the straight line provide an estimate of the quenching cross section of Ar($4p$) atoms by molecular hydrogen. Owing to the proportionality in the actinometric signals issued from $2p_1$ and $2p_9$ states, the quenching cross sections from the two states are equal. HRS spectrometer, 600 mm focal length, 1200 groves/mm grating.

Furthermore, measurements of the ratio of emission intensities (I_{Ar750}/I_{Ar811}) of lines issued from two electronic excited states of argon ($2p_1$ and $2p_9$) were systematically recorded during this experiment. I_{Ar750}/I_{Ar811} remained constant, indicating either that both states are quenched equally by molecular hydrogen, or that Te was constant for the conditions tested in this section.

B. Quenching cross sections

Estimation of the quenching cross sections for the excited states is rather difficult owing to the lack of data concerning collisional diameters corresponding to reactions involving electronic excited state species.

Collision cross sections can be calculated using the collisional diameters of the species in their ground electronic state.[80–82] However, the comparison with the experimental cross sections shows large discrepancies. As a matter of fact, the values for $\sigma_{H\alpha/H_2}$, reported by Bittner *et al.*[27] or Preppernau *et al.*[29] (65 and 58 Å^2, respectively), are seen to be much larger than σ_{H/H_2} (20 Å^2) calculated with the collisional diameters of the ground electronic states. Also, experimental $\sigma_{H\alpha/H_2}$ is seen to be much larger than $\sigma_{H\alpha/H_2}$ calculated with the approximation of Margeneau.[83] Assuming either a linear approach between H and H_2 molecule or a bridged approach,[83] the respective cross sections are 29 and 25.5 Å^2. Concerning σ_{Ar^*/H_2}, again a large discrepancy is observed between our experimental estimation and the value calculated assuming argon in its ground electronic state (26.6 Å^2).[84]

Owing to these large deviations, we chose to calculate the quenching cross sections of excited states H_α and $Ar_{(4p)}$ by H atoms, assuming that the collisional diameters for these reactions are identical to those corresponding to collisions between electronically excited atoms and molecular hydrogen. This assumption appears rather realistic in the case

where the co-linear approach is the only possible configuration, however deviations could appear in the case where the bridged configuration is predominant. On the basis of the assumption of the co-linear approach, the resulting quenching cross section for $\sigma_{H\alpha/H}$ is 46.2 Å^2 (instead of 13 Å^2 for H in the ground state), that for $\sigma_{Ar(4p)/H}$ is 53 Å^2.

With these sets of cross sections, the total quenching factor Q_T can be calculated. The knowledge of its variations as a function of the dissociation yield of molecular hydrogen, pressure, and gas temperature makes possible the estimation of the variations of the relative H-atom mole fraction as a function of operating conditions, in particular as a function of the power density (the pressure and gas temperature vary strongly), and the percentage of methane introduced. However, for reaching absolute variations of H-atom mole fraction, a calibration is needed. Note that owing to the uncertainties on the quenching cross sections, large uncertainties on absolute H-atom mole fractions are expected for large variations of gas temperature or pressure.

VI. OES MEASUREMENTS VERSUS TALIF MEASUREMENTS

From the theoretical analysis, we have shown that *a priori* the use of actinometry could be critical for experimental conditions giving rise to an electron temperature close to 20 000 K associated with a H-atom mole fraction of 3%–5%. For these conditions, the dissociative excitation [reaction (3)] can begin to compete with the direct excitation [reaction (1)] for producing H($n=3$) species. According to calculations, as shown before, the boundary conditions are reached for experimental conditions where the power density is 9 W cm^{-3} (averaged input microwave power=600 W−pressure=2500 Pa.). Our goal now is to compare actinometric signals obtained by OES to fluorescence signals (directly related to ground state H-atom concentration) obtained by TALIF, for these specific experimental conditions.

A. TALIF line shapes and emission line shape analysis

The Doppler broadening of atomic hydrogen spectral lines is large. H-atom and H($n=3$) atom temperatures can be obtained from the measurements of Doppler linewidth $\Delta\lambda_D$ [full width at half maximum (FWHM)] of the fluorescence excitation profile (TALIF) or of the emission profile (OES). These measurements have been performed in this microwave plasma reactor for different operating conditions. In particular, the variations of the temperatures as a function of the percentage of methane added in the feed gas (at 9 W cm^{-3}:600 W and 2500 Pa), and as the function of the power density have been obtained. The results are published in Ref. 32. We demonstrated that the H atoms in the electronic excited state $n=3$ are in thermal equilibrium with the H atoms in the ground electronic state. This is a very good indication that the H($n=3$) excited states are populated directly from the H atoms in the ground electronic state by a direct electron impact ($H+e\rightarrow H(n=3)+e$). As a matter of fact, dissociative excitation process ($H_2+e\rightarrow H(n=3)+H(n=1)+e$) involves energetic electrons (>8 eV). Thus, if it were efficient under these experimental conditions, it would have led to the production of very hot $n=3$ H atoms (with around 4 eV)[85] which are not observed. Consequently, the use of actinometry for H atoms should be valid under the critical set of operating conditions corresponding to 9 W cm^{-3}. However, due to the experimental uncertainties on these measurements and to the difficulty in distinguishing the importance of dissociative excitation relative to the direct excitation as reported by Freund *et al.*,[86] we have preferred to present more results aiming to demonstrate without ambiguity the validity of actinometry at 9 W cm^{-3}.

B. Radial and axial distributions

The H-atom mole fraction can either be derived from TALIF measurements and Eq. (14′) ($x_{H(TALIF)}$), or from OES measurements and Eq. (6′) ($x_{H(OES)}$). From Eq. (6′), it is clear that spatial distributions of $x_{H(OES)}$ can be derived from measurements of $I_{H\alpha}/I_{Ar}$ (the 750.3 nm line is used for argon), knowing the spatial variations of $k_e^{Ar^*}/k_e^{H\alpha}$ (function of Te) and of Q_T (function of Tg).

(1) Measurements of axial distributions of Tg, reported in Ref. 32, allow us to calculate the variations of Q_T. For the domain of variations of Tg (1000–2200 K) corresponding to 9 W cm^{-3}, the spatial variations of Q_T are not exceeding 2%. Then, the spatial variations of Q_T can be neglected.

(2) Concerning the variations of $k_e^{Ar^*}/k_e^{H\alpha}$, the problem is more difficult since Langmuir probes cannot be used to measure electron temperature easily in this kind of environment due to the high pressure. However, as we have shown that both electronic excited states $2p_1$ and $2p_9$ of

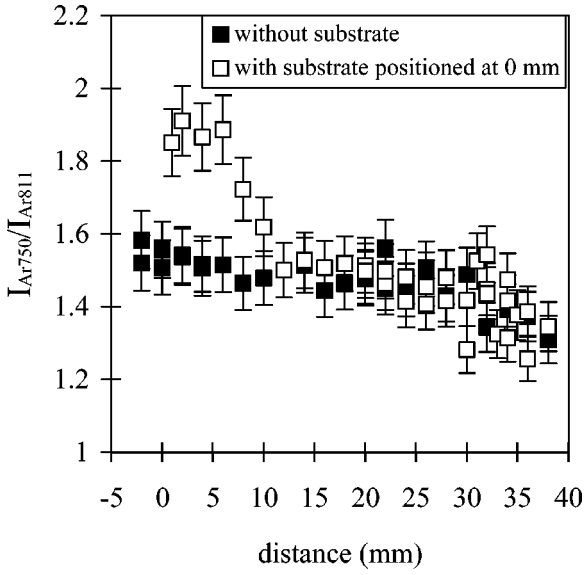

FIG. 6. Axial distributions of emission intensities ratio of argon lines issued from two excited states ($2p_1$ and $2p_9$) (I_{Ar750}/I_{Ar811}) in presence and in absence of a diamond substrate. Discharge conditions: pressure: 2500 Pa, microwave power: 600 W, power density: 9 W cm^{-3}, mixture: 99% H_2+1% Ar. At the real edges of the plasma (location 37–40 mm), the error made on the emission intensity I_{Ar811} is high owing to the fact that the contribution to the signal due to reflexions on the silica reactor becomes as high as that coming directly from the plasma. The values of I_{Ar750}/I_{Ar811} after 37 mm are then not reported in the figure.

argon are excited from the ground electronic state by electron impact and that they are quenched equally by molecular hydrogen, we propose to use the emission intensity ratio of these two lines ($I_{\mathrm{Ar750}}/I_{\mathrm{Ar811}}$) for estimating the spatial evolution of Te. Electron temperature is linked to the emission intensity ratio of the two argon lines by the following relationship:

$$\frac{I_{\mathrm{Ar750}}}{I_{\mathrm{Ar811}}} = F Q_{T\mathrm{Ar}} \frac{\nu_{750} k_e^{\mathrm{Ar}(2p1)}}{\nu_{811} k_e^{\mathrm{Ar}(2p9)}}, \tag{17'}$$

where $k_e^{\mathrm{Ar}(2p1)}$ and $k_e^{\mathrm{Ar}(2p9)}$ are the excitation rate constants for the transitions $\mathrm{Ar}(3p) \rightarrow \mathrm{Ar}(4p)$ (state $2p_1$) (line emitting at 750.3 nm) and $\mathrm{Ar}(3p) \rightarrow \mathrm{Ar}(4p)$ (state $2p_9$) (line emitting at 811.5, nm). The terms ν_{750} and ν_{811} are the de-excitation frequencies for $\mathrm{Ar}(2p_1)$ and $\mathrm{Ar}(2p_9)$ transitions, respectively, and F is an optical device factor. $Q_{T\mathrm{Ar}}$ is the de-excitation term taking into account all the processes of radiative de-excitation and collisional quenching. As the quenching cross sections of both states $2p_1$ and $2p_9$ by atomic and molecular hydrogen are identical, then

$$Q_{T\mathrm{Ar}} = \frac{\{1 + (4.72/3.66) P T^{-1/2} [0.162 \sigma_{\mathrm{Ar}^*/\mathrm{H}_2} x_{\mathrm{H}_2} + 0{,}226 \sigma_{\mathrm{Ar}^*/\mathrm{H}} (1 - x_{\mathrm{H}_2})]\}}{\{1 + P T^{-1/2} [0.162 \sigma_{\mathrm{Ar}^*/\mathrm{H}_2} x_{\mathrm{H}_2} + 0{,}226 \sigma_{\mathrm{Ar}^*/\mathrm{H}} (1 - x_{\mathrm{H}_2})]\}}. \tag{18'}$$

The ratio $k_e^{\mathrm{Ar}(2p1)}/k_e^{\mathrm{Ar}(2p9)}$ depends on Te as shown on Fig. 3 (a Maxwellian distribution for the EEDF was assumed there). Owing to the threshold values of the excited of argon considered here (around 13 eV), and to the fact that the EEDF is actually non-Maxwellian in these experimental conditions[76,89,90] (it is bi-modal), this ratio is linked to the electron temperature of the hot electrons (electrons of the tail of the EEDF) rather than to that of cold electrons. As well, when considering the variations of $k_e^{\mathrm{Ar}(2p1)}/k_e^{\mathrm{H}(n=3)}$ for actinometric measurements, non-Maxwellian EEDF must be used, since again this ratio is governed by ''hot electrons.''

The determination of the electron energy (or of the electron temperature of the hot electrons) could be made *a priori* once the electron excitation cross sections and the non-Maxwellian electron energy distribution function are known. As a matter of fact, calculation of $k_e^{\mathrm{Ar}(2p1)}/k_e^{\mathrm{Ar}(2p9)}$ should be possible. The additional knowledge of calibrated emission intensity ratio $I_{\mathrm{Ar750}}/I_{\mathrm{Ar811}}$ should provide Te according to Eq. (17′). However, the determination of $k_e^{\mathrm{Ar}(2p1)}/k_e^{\mathrm{Ar}(2p9)}$ and $k_e^{\mathrm{Ar}(2p1)}/k_e^{\mathrm{H}(n=3)}$ are strongly linked to the accuracy on the excitation cross sections over the whole range of electron energy considered. This will be discussed in detail elsewhere. At this point, we are only interested by the qualitative evolution of the axial distribution.

Two axial profiles of the emission intensity ratio $I_{\mathrm{Ar750}}/I_{\mathrm{Ar811}}$ are shown in Fig. 6. One corresponds to conditions where no diamond substrate has been introduced in the reactor (the plasma is then like a ball), the second to conditions where a substrate is placed at the 0 mm location (the plasma is like a hemisphere). In absence of substrate, there is almost no variation of $I_{\mathrm{Ar750}}/I_{\mathrm{Ar811}}$ in the plasma except at the plasma edges where a slight decrease is observed. As, in absence of substrate holder, the axial profile is identical to radial profile for reason of spherical symmetry[15] of the plasma, we can conclude that the spatial distribution of the electron energy is flat, except at the edges of the plasma. In presence of a diamond substrate, $I_{\mathrm{Ar750}}/I_{\mathrm{Ar811}}$ (and then Te) is seen to decrease from the surface to the plasma volume where a plateau is observed. At the plasma edges, again a decrease of $I_{\mathrm{Ar750}}/I_{\mathrm{Ar811}}$ is observed. At the plateau and the edges, the values of $I_{\mathrm{Ar750}}/I_{\mathrm{Ar811}}$ are equal to those obtained in the absence of a substrate. The general behavior of the axial variation of $I_{\mathrm{Ar750}}/I_{\mathrm{Ar811}}$ (Te) obtained in the presence of a substrate is in agreement with the evolution of the electron temperature calculated by Grotjohn *et al.*[51] when solving Maxwell equations for this kind of plasma and calculated by Hassouni *et al.*[87]

Owing to these observations, the spatial variations of $k_e^{\mathrm{Ar}^*}/k_e^{H\alpha}$ can be neglected except at the plasma edges where a slight overestimation of $x_{\mathrm{H(OES)}}$ is excepted, when radial profiles or axial profiles in absence of substrate are performed. In the presence of a substrate, neglecting the spatial distributions of $k_e^{\mathrm{Ar}^*}/k_e^{H\alpha}$ may induce a systematic underestimation of $x_{\mathrm{H(OES)}}$ close to the substrate (in particular within the last 10 mm) since the electron temperature is seen to increase in this region.

1. Radial distributions

Radial distributions of relative $I_{H\alpha}/I_{\mathrm{Ar}}$ after Abel inversion and of relative $x_{\mathrm{H(TALIF)}}$ obtained at 9 W cm^{-3}, are reported in Fig. 7. Abel inversion allowed us to compare measurements by TALIF and actinometry made exactly in the same region of the plasma. Similar distributions are observed. $I_{H\alpha}/I_{\mathrm{Ar}}$ very slightly overestimates $(x_{\mathrm{H}})_{\mathrm{OES}}$ at the plasma edge, which is expected. The similarity between these measurements demonstrates without ambiguity the validity of actinometry for these conditions of power density. In addition, it shows that radial analysis of the plasma is possible.

Line-of-sight integrated signals were used most of the time, since Abel inversion is time consuming. We have then estimated the error made when using these integrated measurements. Line-of-sight integrated $I_{H\alpha}/I_{\mathrm{Ar}}$ are compared to Abel inverted $I_{H\alpha}/I_{\mathrm{Ar}}$ in Fig. 8. For a power density of 9 W cm^{-3}, line-of-sight averaged measurements are seen to underestimate by 10% the value of $I_{H\alpha}/I_{\mathrm{Ar}}$ on the axis of the plasma (value obtained with Abel inversion).

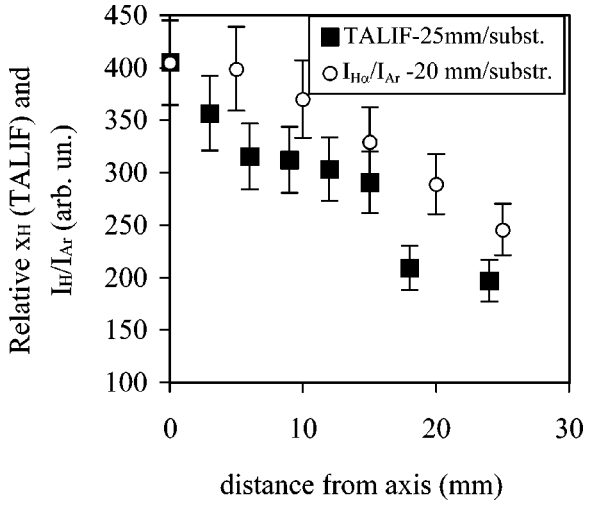

FIG. 7. Radial distributions of relative H-atom mole fraction measured by TALIF and by actinometry after Abel inversion (OES). The variations of the electron temperature are not taken into account in $(x_H)_{OES}$. Discharge conditions: pressure: 2500 Pa, microwave power: 600 W, power density: 9 W cm^{-3}, mixture: 99%H_2+1% Ar.

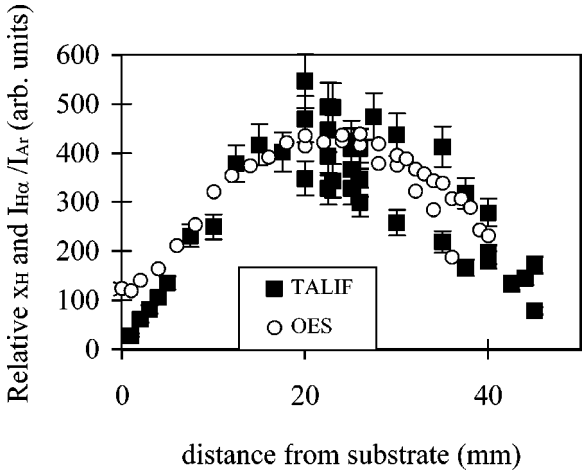

FIG. 9. Axial distributions of relative H-atom mole fraction measured by TALIF and by actinometry with line-of-sight integrated measurements (OES). The variations of the electron temperature are not taken into account in $(x_H)_{OES}$. Discharge conditions: pressure: 2500 Pa, microwave power: 600 W, power density: 9 W cm^{-3}, mixture: 99%H_2+1% Ar.

2. Axial distributions

Axial distributions of relative line-of-sight integrated I_H/I_{Ar} and of a relative $x_{H(TALIF)}$ obtained at 9 W cm^{-3}, are reported in Fig. 9. Again, a very good agreement between these parameters is observed. Owing to the error made during TALIF experiments due to the nonstability of the laser, $(x_H)_{OES}$ does not appear overestimated at the plasma edge. At the interface, the variations of line-of-sight integrated I_H/I_{Ar} and $x_{H(TALIF)}$ are very similar, although $(x_H)_{OES}$ should be underestimated. This indicates that the increase of the electron temperature observed at the plasma/surface interface does not lead to an important change in $k_e^{Ar*}/k_e^{H\alpha}$. Note in addition that, due to the difference in the spatial resolution provided by TALIF measurements (0.5 mm) and by OES (2 mm), a difference in the stiffness of the gradient obtained from the two methods was expected anyway at the interface.

These results again confirm the validity of actinometry at 9 W cm^{-3}. In addition, they show that even if the axial evolution of the electron energy distribution function is not negligible (presence of a ''floating sheath'') (Fig. 6), it does not prevent use of actinometry. This would be the case in the presence of a drastic evolution of the EEDF (strong increase in the electron temperature as it occurs, for instance, near a cathodic sheath[7]).

As a conclusion, we can state that at 9 W cm^{-3}, H($n=3$) atoms are mainly produced by electron impact from their electronic ground state. Actinometry can then be used for measuring axial and radial profiles under discharge conditions corresponding to diamond deposition (in the absence of substrate biasing, of course), once the power density is higher than 9 W cm^{-3}.

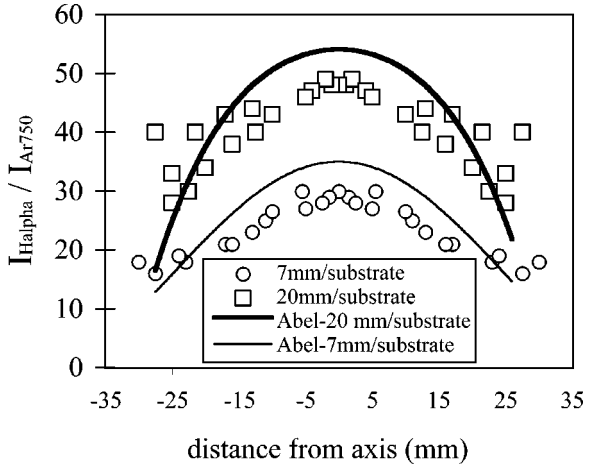

FIG. 8. Line-of-sight integrated and Abel inverted measurements of $I_{H\alpha}/I_{Ar}$ for two axial locations in the plasma. Discharge conditions: pressure: 2500 Pa, microwave power: 600 W, power density: 9 W cm^{-3}, mixture: 99%H_2+1% Ar.

C. Variations of $I_{H\alpha}/I_{Ar}$ (OES) and x_H (TALIF) as a function of the percentage of methane

A comparison of the relative variations of $(x_H)_{OES}$ and $(x_H)_{TALIF}$ as the percentage of methane in the feed gas is increased at up to almost 6% is presented in Fig. 10. All the measurements are performed at 20 mm from the substrate (plasma volume) and at a power density of 9 W cm^{-3}. As $I_{H\alpha}/I_{Ar}$ measurements were line-of-sight integrated, then the volumes of the plasma analyzed by TALIF and OES were different.

The variations of $(x_H)_{OES}$ and $(x_H)_{TALIF}$ versus the percentage of methane are very similar. As a very small amount of methane is introduced (0.25%–0.5%), both $(x_H)_{TALIF}$ and $(x_H)_{OES}$ increase. This behavior is attributed to a slight increase in the electron density owing to the presence in the gas of hydrocarbon species, in particular C_2H_2 which is the main hydrocarbon species under these conditions[87] and which have a lower ionization threshold (10 eV)[88] than

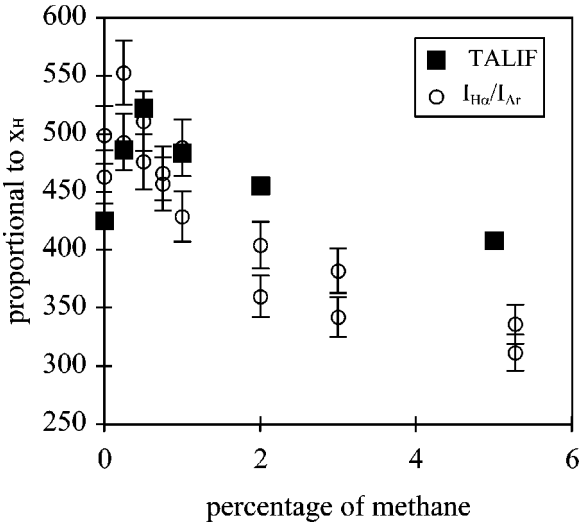

FIG. 10. Relative H-atom mole fraction measured by TALIF and OES (actinometry with integrated line of sight) vs the percentage of methane introduced in the feed gas. Discharge conditions: pressure: 2500 Pa, microwave power: 600 W, power density: 9 W cm^{-3}, mixture: $99-x\%$ $H_2+1\%$ Ar $+x\%$ CH_4.

atomic (13.6 eV) and molecular (15.5 eV) hydrogen. As a matter of fact, it cannot be attributed to an increase in *Te* since I_{Ar750}/I_{Ar811} was seen to remain constant as a function of the percentage of methane. After this increase due to ionization processes, a decrease of $(x_H)_{OES}$ and $(x_H)_{TALIF}$ is observed. It is attributed to the consumption of H atoms owing to the chemical reactions involving methane which are thermally activated. This decrease has only been observed in conditions of low power density where a gas temperature of 2200 K is reported. At higher power density, higher gas temperatures are reported and, although the increase due to ionization processes is still observed, it is not the case for the decrease observed at a higher percentage of CH_4 (see Fig. 12). At higher gas temperature and higher H-atom mole fraction, even if H atoms are involved for dissociation of methane, the net balance does not show it.

Although showing very similar evolution, $(x_H)_{OES}$ decreases faster than $(x_H)_{TALIF}$ does. This behavior is attributed to the fact that the TALIF measurements are made locally on the axis of the plasma [cylinder parallel to the surface: 0.5 mm in diameter and 1 mm long (0.2 mm^3)], while OES measurements are line-of-sight averaged [on a cylinder 2 mm in diameter and 50 mm long (157 mm^3)].

As seen above, the depletion of the H-atom mole fraction owing to the introduction of methane is a characteristic of low gas temperature and low H-atom mole fraction (see Fig. 12).[30] The higher the gas temperature and the H-atom mole fraction, the less the H-atom depletion. As a consequence, different behavior is expected at the plasma center and at the edges. Line-of-sight averaged measurements involve emission of species coming from different plasma shells. Each shell is characterized by a given H-atom mole fraction and a given gas temperature. In particular, the outer shells are characterized by lower H-atom mole fraction and *Tg* than the inner shells. Then, the depletion of the H atoms within the outer shell is expected to be larger than within the inner shells. Consequently, we can understand why line-of-sight averaged measurements exhibit larger depletion (25%) than the local measurements made on the axis of the plasma by TALIF (20%) do, as methane is introduced in the reactor.

Keeping in mind these effects, we consider that the variations of the H-atom mole fraction measured by TALIF and OES are similar enough to conclude that these results constitute an additional proof for the validity of actinometry for H atoms under this set of experimental conditions corresponding to 9 W cm^{-3}.

VII. VARIATIONS OF THE ELECTRON ENERGY AND THE H-ATOM MOLE FRACTION AS A FUNCTION OF THE METHANE PERCENTAGE AND THE AVERAGED POWER DENSITY

In order to draw the domain of validity of actinometry, in this section we estimate the variations of *Te* and x_H as a function of the power density and of the percentage of methane introduced in the feed gas, since these parameters are keys for chemical vapor deposition (CVD) diamond deposition plasma reactors. For reaching the variations of *Te* (or if possible the EEDF), either experimental measurements of the ratio of emission intensities of the two transition lines of argon discussed above (I_{Ar750}/I_{Ar811}) or calculations are made.

The variations of the emission intensities ratio I_{Ar750}/I_{Ar811} as a function of the percentage of methane and for different microwave power densities have been measured. No variation was observed as the methane is varied from 0% to almost 6%, whatever the power density. This has been confirmed by calculations of the electron energy distribution function (EEDF) as a function of the percentage of methane assuming a non-Maxwellian distribution.[76,89,90] On the opposite, $I_{Ar750\,nm}/I_{Ar811}$ decreases as the power density increases from 9 to 33 W cm^{-3}, indicating a decrease in *Te* (Fig. 11). This behavior has been also confirmed by calculations[17] (Fig. 11).

We can then conclude that, as far as the electron temperature is concerned, actinometry will be valid for a very large range of diamond deposition conditions. As a matter of fact, we have shown that the upper limit for *Te* (20 000 K) is obtained at relatively low power density (less than 9 W cm^{-3}). As the power density is increased, both power and pressure are increased. The consequence is an increase in the electron collision frequency and then in the electron-neutrals energy transfer, therefore *Te* decreases. Consequently, the limitation due to the electron temperature will not be a problem when working at high power densities (>9 W cm^{-3}). As high power densities are generally used for growing diamond, actinometry applied for estimating H-atom mole fraction will be valid most of the time under diamond deposition conditions. To be rigorous, according to Fig. 4, we have to verify that H-atom mole fraction is not decreasing with the power density.

The results presented in Fig. 12 show that $I_{H\alpha}/I_{Ar}$ is much higher for power densities of 15 and 20 W cm^{-3} than for a power density of 9 W cm^{-3}, indicating an increase of H-atom mole fraction with power density. We have shown previously[32] that the gas temperature increases with the

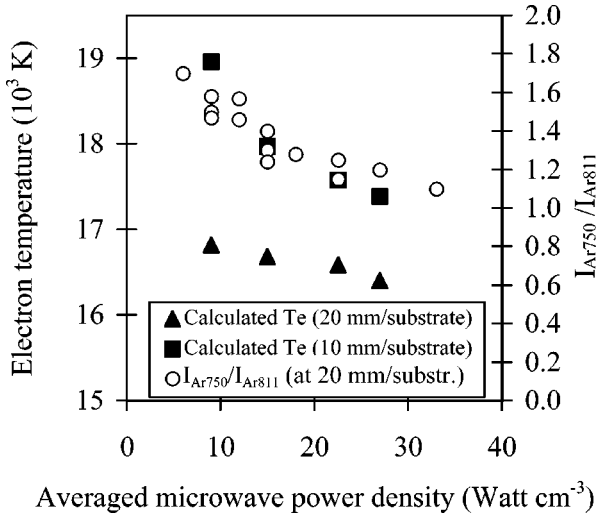

FIG. 11. Calculated electron temperature (obtained from 1D diffusive H_2 plasma model) and emission intensities ratio I_{Ar750}/I_{Ar811} vs the averaged input microwave power density.

power density (it increases from 2200 to around 2800 K as power density increases from 9 to 20 W cm^{-3}), and we just saw that *Te* decreases; we can then partly attribute the increase in x_H with power density to thermal dissociation.

Therefore, we can state to an apparent absence of upper limit value of power density for using actinometry for estimating H-atom mole fraction, for conditions typical for diamond deposition. Nevertheless, we can imagine that too high power density ($>150-200$ W cm^{-3}) may bring other phenomena (formation of an atomic gas, autoabsorption,...), which have not been analyzed in detail in this article. Consequently, precautions may be taken at these very high power densities. In addition, the determination of absolute H-atom mole fraction as a function of power density on the basis of actinometric measurements will remain difficult, owing to the large uncertainties on the electronic excited state quenching cross sections.

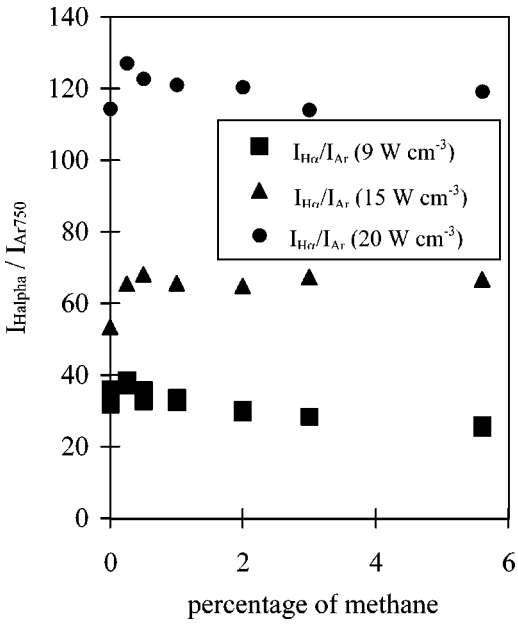

FIG. 12. Emission intensities ratio $I_{H\alpha}/I_{Ar}$ vs the percentage of methane introduced in the feed gas, and for two different microwave power densities.

When adding methane to the reactive plasma, both *Te* and T_g[32] (gas temperature) are unchanged. As shown on Fig. 10, x_H slightly decreases (by 25%) as methane is increased at 9 W cm^{-3}, while it remains constant for higher power densities as shown in Fig. 12. As a consequence, the validity of actinometry is not altered by the introduction of methane (up to 6% at least), and the predominant path for producing H($n=3$) is the direct impact of electrons on ground state H atoms.

VIII. CONCLUSION

As a conclusion, the domain of validity of actinometry has been determined for typical discharge conditions used for growing diamond.

A relationship allowing the determination of the H-atom mole fraction from the knowledge of a ratio of emission intensities of lines issued from H($n=3$) and from Ar($4p$), has been established. A theoretical approach has shown that the relation is valid for conditions characterized by an electron temperature less than 20 000 K associated with a H-atom mole fraction of around 2%–5%. The calculations, based on a 1D diffusive H_2 plasma flow model, showed than this boundary is reached for experimental conditions corresponding to a power density of 9 W cm^{-3}, i.e., a power of 600 W and a pressure of 2500 Pa.

For these conditions corresponding to 9 W cm^{-3}, the validity of actinometry has been established on the bases of (i) the equality between the H($n=3$) atom temperature and that of ground state H atoms, (ii) the similarities between axial and radial distributions of the relative H-atom mole fraction deduced from TALIF and OES, and (iii) the similarity in the behavior of the H-atom mole fraction deduced from TALIF and OES when adding methane in the feed gas.

Calculations and experiments demonstrated, finally, that the electron temperature decreases while the H-atom mole fraction increases as the microwave power density increases. Then, the direct excitation of H($n=3$) is favored at higher microwave power density. They also showed that *Te* and x_H remain in the same magnitude as methane is introduced up to 6% in hydrogen, making the validity of actinometry unaltered as methane is introduced in the feed gas.

As a conclusion, actinometry can be applied to measurements of H-atom mole fraction under diamond deposition conditions at power densities higher than 9 W cm^{-3}. These conditions are widely used for deposition of diamond.

Estimations of the variations of H-atom mole fractions as a function of the operating conditions require the knowledge of the variation of the electron temperature and of the quenching factor. The accuracy of the quenching factor depends on the measurements of the gas temperature and of the accuracy of the quenching cross sections of electronic excited H and Ar atoms by ground state atomic and molecular hydrogen. The quenching cross section of H($n=3$) by molecular hydrogen was already known and this work allowed us to estimate that of $2p_1$ and $2p_9$ states of argon by mo-

lecular hydrogen. However, very little is known on the quenching cross sections of electronic excited H and Ar atoms by ground state H atoms. As their contributions increase with the dissociation yield, an accurate estimation of H-atom density at high power density will be difficult. A calibration of the optical system devices used in different laboratories should nevertheless allow a quantitative comparison in the performances of the diamond deposition reactors.

We have also discussed the use of the emission intensity ratio of two lines issued from excited states of argon atoms for estimating the variations of the two temperatures characterizing the electrons of the plasma (hot and cold electrons).

ACKNOWLEDGMENTS

This work was financially supported by DRET and EC (BRITE EURAM II and III). The authors thank J. C. Cubertafon, J. P. Booth, and Y. Breton for their contributions in TALIF measurements and OES measurements, respectively. Thomas Owano is gratefully thanked for English language corrections.

[1] J. W. Coburn and M. Chen, J. Appl. Phys. **51**, 3134 (1980).
[2] R. D'Agostino, F. Cramarossa, S. de Benedictis, and G. Ferraro, J. Appl. Phys. **52**, 1259 (1981); R. D'Agostino, V. Colaprico, and F. Cramarossa, Plasma Chem. Plasma Process. **1**, 365 (1981).
[3] A. D. Richards, B. E. Thompson, K. D. Allen, and H. H. Sawin, J. Appl. Phys. **62**, 792 (1987).
[4] A. Ricard, *Plasma Réactifs*, edited by Société Française du Vide, 1995, Chap. 4.
[5] R. A. Gottscho and V. M. Donnelly, J. Appl. Phys. **56**, 245 (1984).
[6] R. E. Walkup, K. L. Saenger, and G. S. Selwyn, J. Chem. Phys. **84**, 2668 (1986).
[7] A. Gicquel, P. Saillard, S. Piétré, M. Cappelli, and J. Amouroux, Proceedings of the 10th International Symposium on Plasma Chemistry, edited by U. Ehlemann, H. G. Lergon, and K. Wiesmann, 1991 (unpublished), Vol. 2, pp. 2.1–4.1.
[8] E. Vietzke, V. Philipps, K. Flaskamp, J. Winter, S. Veprek, and P. Koidl, in Ref. 7, Vol. 3, pp. 3.1–1.1.
[9] Status on applications of diamond and diamondlike materials: an emerging technology. National Materials Advisory board. Committee on superhard materials, Chairman J. D. Venables (1990).
[10] N. Setaka, J. Mater. Res. **4**, 664 (1989).
[11] B. B. Pate, Surf. Sci. Lett. **165**, 83 (1986).
[12] F. G. Celii and J. E. Butler Appl. Phys. Lett. **54**, 1031 (1989).
[13] E. A. Evans and J. C. Angus, Diamond Relat. Mater. **5**, 200 (1996).
[14] W. L. Hsu, J. Appl. Phys. **72**, 3102 (1992).
[15] A. Gicquel, K. Hassouni, S. Farhat, Y. Breton, C. D. Scott, M. Lefebvre, and M. Pealat Diamond Relat. Mater. **3**, 581 (1994).
[16] C. D. Scott, S. Farhat, A. Gicquel, K. Hassouni, and M. Lefebvre, AIAA 93-3226, 24th Plasmadynamics and Lasers Conference. July 6–9, 1993, Orlando, FL, July 6–9; C. D. Scott, S. Farhat, A. Gicquel, K. Hassouni, and M. Lefebvre, ThermoPhysics and Heat Transfer **10**, 426 (1996).
[17] K. Hassouni, S. Farhat, C. D. Scott, and A. Gicquel, J. Phys. III (France) **6**, 1229 (1996).
[18] S. O. Hay, W. Roman, and M. B. Colket III, J. Mater. Res. **5**, 2387 (1990).
[19] D. G. Goodwin, J. Appl. Phys. **74**, 6895 (1993).
[20] J. Harris and A. M. Weiner, J. Appl. Phys. **74**, 1022 (1993); S. J. Harris, A. M. Weiner, and R. J. Blint, Combust. Flame **65**, 177 (1986).
[21] B. J. Wood and H. Wise, J. Phys. Chem. **65**, 1976 (1961); **66**, 1049 (1962).
[22] H. Wise and B. J. Wood, Adv. At. Mol. Phys. **3**, 291 (1967).
[23] J. Wood and H. Wise, J. Chem. Phys. **66**, 1049 (1962).
[24] B. Halpern and D. E. Rosner, Trans Faraday Soc. **160**, 1883 (1978).
[25] F. G. Celii and J. E. Butler, Appl. Phys. Lett. **54**, 1031 (1989).
[26] F. G. Celii, H. R. Thorsheim, J. E. Butler, L. S. Plano, and J. M. Pinneo, J. Appl. Phys. **68**, 3814 (1990).
[27] J. Bittner, K. Kohse-Höinghaus, and U. Meier, Th. Just. Chem. Phys. Lett. **143**, 571 (1988).
[28] M. Chenevier, J. C. Cubertafon, A. Campargue, and J. P. Booth, Diamond Relat. Mater. **3**, 587 (1994).
[29] B. L. Preppernau, K. Pearce, A. Tserepi, E. Wurzberg, and T. A. Miller, Chem. Phys. **196**, 371 (1995).
[30] A. Gicquel, M. Chenevier, and M. Lefebvre, in *Handbook of Industrial Diamonds and Diamond Films*, Chap. 19, edited by M. Prelas, G. Popovicci, and K. Bigelow (Marcel Dekker, New York, 1998), p. 739.
[31] M. Chenevier, A. Gicquel, and J. C. Cubertafon, in *Proceedings of the Third International Conference on the Applications of Diamond Films and Related Materials* (ADC'95), edited by Y. Tzeng, M. Yoshikawa, M. Murakawa, and A. Feldman (Elsevier, Gaithersburg, 1995), p. 305.
[32] A. Gicquel, M. Chenevier, Y. Breton, M. Petiau, J. P. Booth, and K. Hassouni J. Phys. III **6**, 1167 (1996).
[33] A. Mucha, D. L. Flamm, and D. E. Ibbotson, J. Appl. Phys. **65**, 3448 (1989).
[34] T. Lang, J. Stiegler, Y. von Kaenel, and E. Blank, Diamond Relat. Mater. **5**, 1171 (1996).
[35] A. Rousseau, A. Granier, G. Gousset, and P. Leprince, J. Phys. D **27**, 1412 (1994).
[36] L. St. Onge and M. Moisan, Plasma Chem. Plasma Process. **14**, 87 (1994).
[37] D. K. Milne, P. John, I. C. Drummond, P. G. Roberts, M. G. Jubber, and J. I. B. Wilson, Diamond Relat. Mater. **2**, 1430 (1993).
[38] S. E. Savas, Appl. Phys. Lett. **48**, 1042 (1986).
[39] J. Ropcke and A. Ohl, Contrib. Plasma Phys. **34**, 575 (1994).
[40] K. Ito, N. Oda, Y. Hatano, and T. Tsuboi, Chem. Phys. **17**, 35 (1976).
[41] K. H. Chen, M. C. Chuang, C. M. Penney, and W. F. Banhollzer, J. Appl. Phys. **71**, 1485 (1992).
[42] A. Gicquel, K. Hassouni, Y. Breton, M. Chenevier, and J. C. Cubertafon, Diamond Relat. Mater. **5**, 366 (1996).
[43] S. J. Buckmann and A. V. Phelps, JILA Informations Center Report No. 27, University of Colorado Boulder, 1985 (unpublished).
[44] H. Tawara, Y. Itikawa, H. Nishimura, and M. Yoshino, J. Phys. Chem. Ref. Data **19**, 3 (1990).
[45] R. K. Janev, W. D. Langer, K. Evans, Jr., and D. E. Post, Jr., in *Elementary Process in Hydrogen Plasma* (Springer, Berlin, 1987), p. 25.
[46] P. Laborie, J. M. Rocard, and J. A. Rees, *Tables de Sections Efficaces Électroniques et Coefficients Macroscopiques 1 Hydrogène et Gaz Rares* (Dunod, Paris, 1968); I. P. Zapesochnyi, and P. V. Feltsan, Opt. Spectrosc. U.R.S.S., English translation **20**, 291 (1966).
[47] M. A. A. Clyne, P. B. Monkhouse, and D. W. Setser, Chem. Phys. **28**, 447 (1978).
[48] N. Sadeghi and D. W. Setser, Chem. Phys. **95**, 305 (1985).
[49] W. L. Fite, R. T. Brackmann, D. G. Hummer, and R. F. Stebbings, Phys. Rev. **116**, 363 (1959).
[50] W. E. Lamb, Jr. and R. C. Retherford, Phys. Rev. **79**, 549 (1950).
[51] W. Tan and T. Grotjohn, J. Vac. Sci. Technol. A **12**, 1216 (1994).
[52] M. Glass-Maujean, Phys. Rev. Lett. **62**, 144 (1989).
[53] V. Dose and A. Richard, J. Phys. B **14**, 63 (1981).
[54] V. Dose and W. Hett, J. Phys. B **7**, 454 (1974).
[55] V. Dose, Comments At. Mol. Phys. **5**, 151 (1976).
[56] S. R. Ryan, S. J. Czuchlewski, and M. V. McCusker, Phys. Rev. A **16**, 1892 (1977).
[57] A. C. Roach and P. J. Kuntz, J. Chem. Phys. **84**, 822 (1986).
[58] R. S. Kass and W. L. Williams, Phys. Rev. **7**, 10 (1973).
[59] Y. Lebedev, in *Proceedings of the Workshop on Microwave Plasma and Applications*, Zvenigorod, Russia, Sept. 5–8, 1994, edited by (Moscow Physical Society, Moscow, 1995), p. 121.
[60] Holstein, Phys. Rev. **83**, 1159 (1951).
[61] L. L. Alves, G. Gousset, and C. M. Ferreira, J. Phys. D **25**, 1713 (1992).
[62] R. C. Cheshire, V. Kornas, H. F. Döbele, K. Donnelly, D. Dowling, W. G. Graham, T. Morrow, and T. O'Brien, Proceedings of the Twelfth European Sectional Conference on the Atomic and Molecular Physics of Ionized Gases, 1994 (unpublished), Vol. E, p. 474.
[63] J. K. Ballou and C. C. Lin, Phys. Rev. A **8**, 1797 (1973).
[64] P. Ségur and M. C. Bordage, Proceedings of the XIXth International Conference on Phenomena in Ionized Gases, invited paper, edited by U. J. Zigman Belgrade, 1989 (unpublished), p. 86.
[65] T. Sawada, J. E. Purcell, and A. E. S. Green, Phys. Rev. A **4**, 193 (1971).
[66] C. R. Lloyd, E. Weigold, P. J. O. Tuebner, and S. T. Hood, J. Phys. B **5**, 1712 (1972).
[67] O. Krogh, T. Wicker, and B. Chapmann J. Vac. Sci. Technol. B **4**, 1292 (1986).
[68] H. A. Hyman, Phys. Rev. A **18**, 441 (1978).
[69] F. A. El Yachkouri, thesis, Université d'Orléans, 1995.

[70] W. L. Wiese, M. W. Smith, and B. M. Miles, in *Atomic Transition Probabilities, NSRDS NBS* (U.S. Government Printing Office Washington, DC, 1969), Vol. 2, p. 22.
[71] L. G. Piper, J. E. Velazco, and D. W. Setser, J. Chem. Phys. **59**, 3323 (1973).
[72] J. E. Velazco, J. H. Kolts, and D. W. Setser, J. Chem. Phys. **69**, 4357 (1978).
[73] E. H. Fink, D. Wallach, and C. B. Moore, Chem. Phys. **56**, 3608 (1972).
[74] K. Hassouni, M. Capitelli, S. Farhat, C. D. Scott, and A. Gicquel, Surf. Coat. Technol. **97**, 495 (1997).
[75] M. Gordon, *Handbook of Industrial Diamonds and Diamond Films*, edited by M. Prelas, G. Popovicci, and K. Bigelow (Marcel Dekker, New York, 1997), Chap. 15, p. 631.
[76] M. H. Gordon and U. Kelkar, Phys. Plasma Controlled Fusion **3**, 407 (1996).
[77] V. Schulz-von der Gathen and H. F. Döbele, Plasma Chem. Plasma Process. **16**, 461 (1996).
[78] J. Bittner, K. Kohse-Höinghaus, U. Meier, S. Kelm, and Th. Just, Combust. Flame **71**, 41 (1988).
[79] J. Tung, A. Tang, G. Salamo, and F. Chan, J. Opt. Soc. Am. B **3**, 837 (1986).
[80] M. J. Kushner, J. Appl. Phys. **63**, 2532 (1988).
[81] Y. Matsui, A. Yuuki, N. Morita, and K. Tachibana, Jpn. J. Appl. Phys., Part 1 **26**, 1575 (1987).
[82] J. O. Hirschfelder, C. F. Curtis, and R. B. Bird, in *Molecular Theory of Gases and Liquids* (Wiley, New York, 1954), p. 1081.
[83] H. Margeneau, Phys. Rev. **66**, 303 (1944); **64**, 131 (1943); J. O. Hirschfelder, C. F. Curtis, and R. B. Bird, in Ref. 82, p. 1081.
[84] J. E. Velazco, J. H. Kolts, and D. W. Setser, J. Chem. Phys. **69**, 4357 (1978).
[85] L. Tomasini, thesis, l'Université Paris XI, 1996.
[86] R. S. Freund, J. A. Schiavone, and D. F. Brader, J. Chem. Phys. **64**, 1122 (1976).
[87] Kh. Hassouni, O. Leroy, S. Farhat, and A. Gicquel, J. Plasma Chem. Plasma Process. (accepted 1998).
[88] H. Tawara, Y. Itikawa, H. Nishimura, H. Tanako, and Y. Nabamwa, Collision Data Involving Hydrocarbon Molecules, NIFS-DATA6-Research Report (July 1990), Nagoya Japan.
[89] C. R. Koemtzopoulos, D. J. Economou, and R. Pollard, Diamond Relat. Mater. **2**, 25 (1993).
[90] M. Capitelli, G. Colonna, K. Hassouni, and A. Gicquel, Plasma Chem. Plasma Process. **16**, 153 (1996).